10. SCIAMACHY's View of the Earth's Atmosphere

Expectations were high when SCIAMACHY was launched in March 2002. The scientific user community was eagerly awaiting first measurement data and results. So far, as outlined in the previous chapters, the instrument has fully met its requirements and goals. Since summer 2002, a continuous stream of high quality data has been acquired at the ground stations and disseminated for further processing, scientifically and operationally. Although the time since launch is still insufficient to fully exploit SCIAMACHY's scientific capabilities, the results obtained so far provide new insights into the Earth-atmosphere system. The layered approach described in chapter 1.3, from Earth's surface to the top of the atmosphere and even beyond into the solar environment, permits exploration of many aspects of atmospheric physics and chemistry. SCIAMACHY has already significantly contributed to these areas. What is presented in the following tour through the atmosphere will highlight some of the most spectacular findings. It is however only a small subset of the existing material. Many scientific groups at various institutes in Europe and abroad are involved in the scientific analysis of the data. Their efforts ensure the timely availability of excellent results. The interested reader is further referred to the internet resources:

http://www.dlr.de/dlr/news/sciamachy/
http://envisat.esa.int/
http://www.sciamachy.de/
http://www.sciamachy.org/
http://wdc.dlr.de/
http://www.iup.physik.uni-bremen.de/
http://satellite.iup.uni-heidelberg.de/
http://www.temis.nl/
http://gse-promote.org/

where SCIAMACHY data products, scientific results and related detailed information about our atmosphere can be found.

10.1 Troposphere

SCIAMACHY measurements provide information on a number of tropospheric constituents as solar radiation penetrates the atmosphere down to the surface. Here the atmospheric conditions define mankind's environment in many ways. Our civilisation generates significant stress upon the troposphere. Pollution and smog are increasing and become global problems in a more and more industrialised world. SCIAMACHY has shown that air quality is not only an issue in densely populated regions but also in remote sites, e.g. above the oceans.

Nitrogen Dioxide – NO_2

The highly variable NO_2 is one of the key species in the troposphere. It catalyses ozone production, contributes to acidification and also adds to radiative forcing. The main sources of NO_2 are anthropogenic in origin, e.g. industry, power plants, traffic and forced biomass burning. Other but slightly less important origins comprise natural biomass burning, lightning and microbiological soil activity. NO_2 emissions have increased by more than a factor of 6 since pre-industrial times with concentrations being highest in large urban areas.

Global monitoring of tropospheric NO_2 emissions is a crucial task. SCIAMACHY's predecessor GOME has already demonstrated the unique ability to monitor tropospheric air pollution. Fig. 10-1 shows a global survey of tropospheric NO_2 as seen by SCIAMACHY. Due to its higher spatial resolution (60 x 30 km^2 as compared to 320 x 40 km^2 for GOME), SCIAMACHY enables us performing very detailed observations of polluted regions. This is obvious in fig. 10-2 where industrialised regions of North America, Europe and China are displayed. As a result of these new datasets, individual cities and even large power plants can be identified in the measurements (e.g. *Beirle et al. 2004*, *Richter et al. 2005*).

Particularly interesting are the studies concerning the global trend in NO_2 concentrations as depicted in fig. 10-3 *(Richter et al. 2005)*. By combining SCIAMACHY results with those of previous missions, e.g. GOME, it is possible to investigate how the tropospheric NO_2 load has changed over the past decade. For Central Europe and the East Coast of the United States concentrations slightly decreased or remained constant while China developed into a strong NO_2 source. The inset in fig. 10-3 also demonstrates how well SCIAMACHY and GOME match; NO_2 vertical columns of both instruments perfectly overlap around the turn of the year 2002. The periodic trend in NO_2 columns each year can mainly be attributed to seasonal variations in energy consumption.

This type of data provides much improved constraints for attempts to quantify emission strengths by inverse modelling and facilitates derivation of independent top-down estimates of emissions not only on a country-by-country basis but even on regional

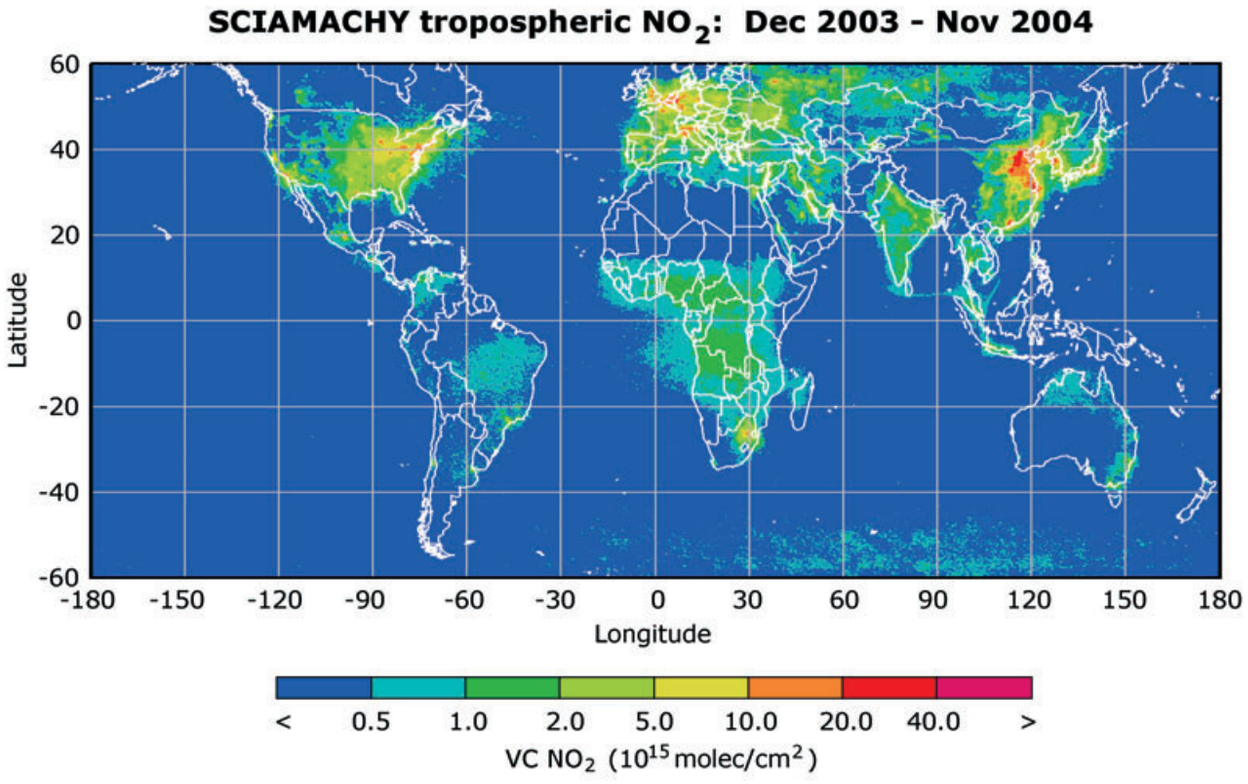

Fig. 10-1: Global survey of tropospheric NO_2 for December 2003 to November 2004. Clearly visible are the industrialised regions in the northern hemisphere and regions of biomass burning in the southern hemisphere. (image: A. Richter, IUP-IFE, University of Bremen)

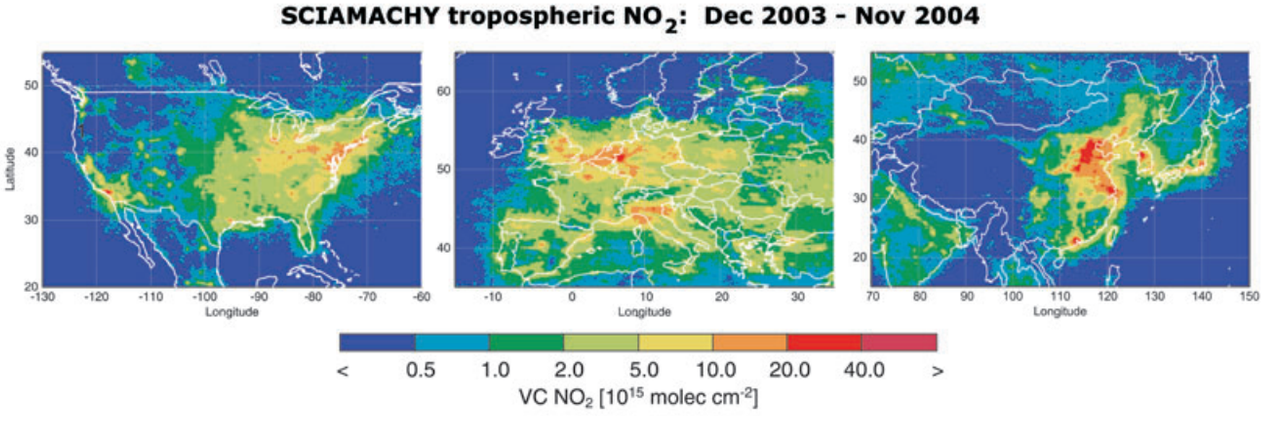

Fig. 10-2: Mean tropospheric NO_2 densities over Europe, the United States and China between December 2003 and November 2004. (image: A. Richter, IUP-IFE, University of Bremen)

scales. The increased spatial resolution and high sensitivity of the measurements even allows the detection of localised sources down to the level of frequently used ship routes *(Richter et al. 2004)*, as illustrated in fig. 10-4.

Sulphur Dioxide – SO_2

SO_2 is another pollutant that can be observed using SCIAMACHY spectra. Sources of SO_2 are combustion of sulfur rich coal and other fossil fuels or volcanic eruptions including degassing. Although SO_2 emissions have been reduced significantly over the last decades, clear signals can be detected over the Eastern United States and in particular the polluted areas of China (fig. 10-5). As in the case of NO_2, the improved spatial resolution facilitates source identification and makes the data set an interesting new data source for air quality measurements.

Volcanoes are a natural source of SO_2 emissions. Since the start of SCIAMACHY's routine observations

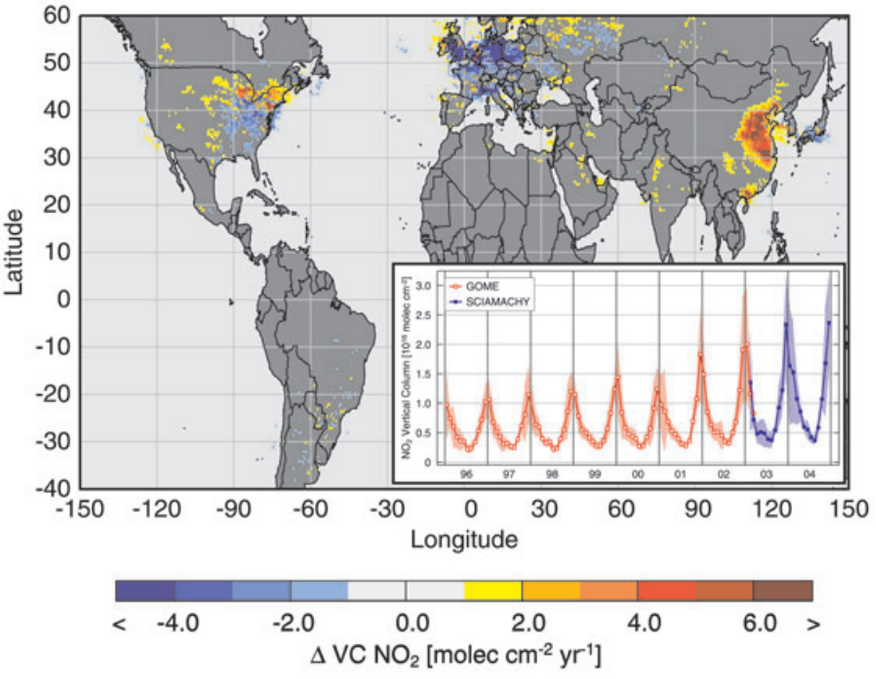

Fig. 10-3: Change in global tropospheric NO_2 concentrations from 1996-2002. The inset illustrates how NO_2 concentrations have risen in China from 1996-2004. The trend analysis uses data from GOME (1996-2002) and SCIAMACHY (2003-2004). While 'old' industrialised countries were able to stop the increase of NO_2 emissions, the economical growth in China turns out to be a strong driver for pollution. (image: A. Richter, IUP-IFE, University of Bremen)

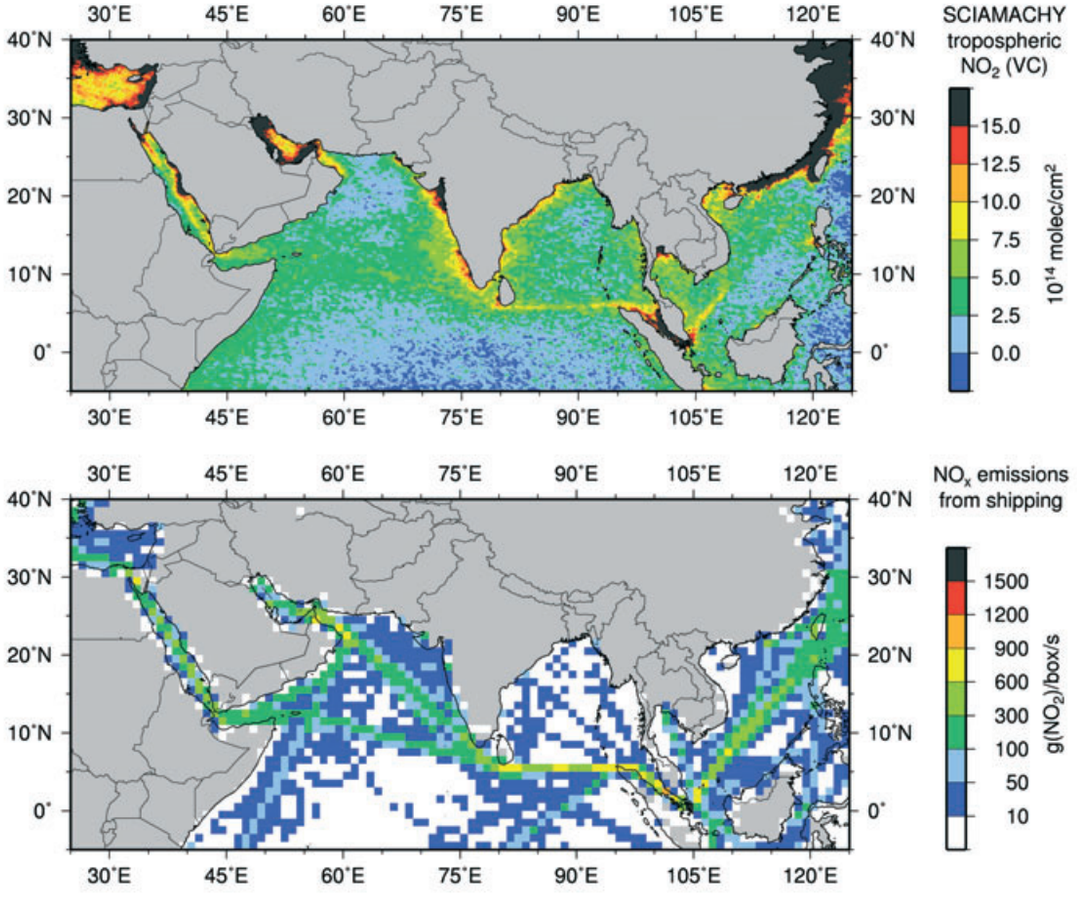

Fig. 10-4: NO_2 densities over the Indian Ocean and the Red Sea as derived from measurements between August 2002 and April 2004 (top). The highly frequented ship routes from Eastern Asia to the Suez Canal can be clearly seen. Along the coast lines strong NO_2 concentrations are the result of urban industrialised areas. In the lower panel the NO_x emissions associated with shipping based on emission inventories is depicted. (image: A. Richter, IUP-IFE, University of Bremen)

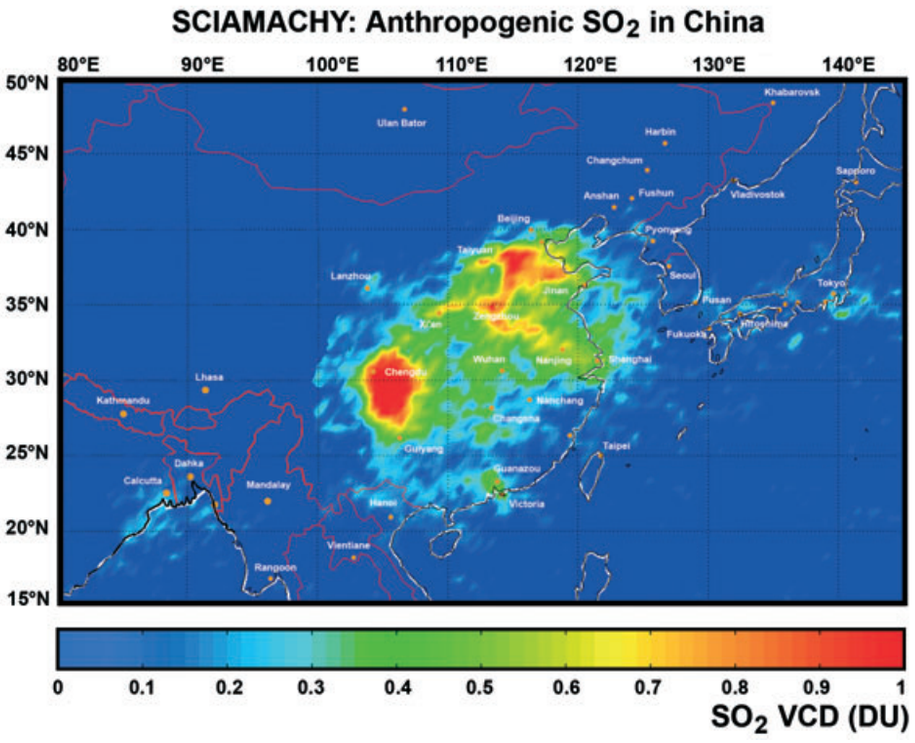

Fig. 10-5: Average SO_2 column densities over eastern China during the year 2003. SCIAMACHY's improved spatial resolution permits to identify localised emissions due to anthropogenic activities. (image: M. Van Roozendael, IASB-BIRA)

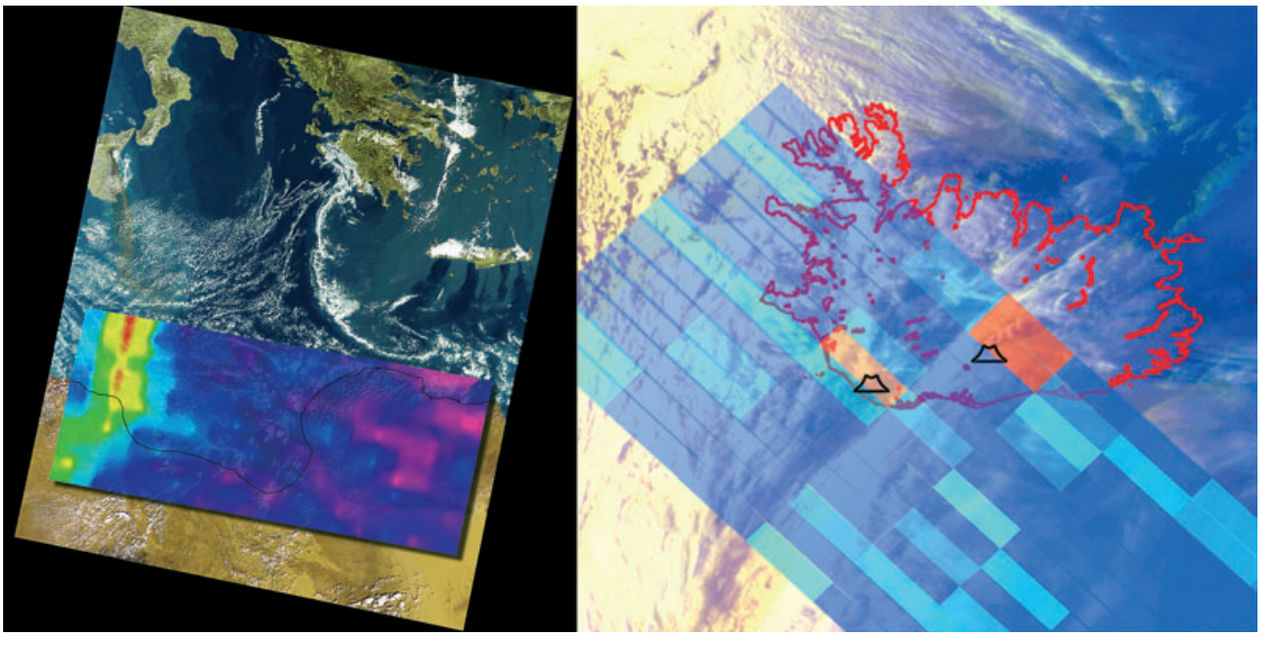

Fig. 10-6: Two European volcanic eruptions with obvious SO_2 emissions: Mt. Etna (left) and Grimsvötn (right). The SCIAMACHY nadir measurement of Mt. Etna is overlayed on a MERIS image showing that the plumes of SO_2 and visible ash match well. In the Iceland image (right) detected SO_2 emission at Grimsvötn is indicated by the red pixel. The second faint SO_2 enhancement in the south of Iceland is caused by the Katla volcanoe. The underlying visible image stems from AVHRR/NOAA-12. (images: Mt. Etna – DLR-IMF, Iceland – DLR-DFD and IUP-IFE, University of Bremen)

a few of the several hundred existing active volcanoes have been erupting and overpassed by ENVISAT. In October 2002, Mt. Etna on the island of Sicily entered an explosive phase. The rectangular overlay in fig. 10-6 (left panel) represents a SCIAMACHY nadir measurement displaying SO_2 emissions which match well with the ash plume visible in a simultaneously obtained image by MERIS on ENVISAT. Early in November 2004 the Grimsvötn, located in Iceland's Vatnajöküll glacier area, began a series of violent eruptions. An ash plume was released which also contained noticeable amounts of sulphur dioxide detect-

ed by SCIAMACHY (fig. 10-6 right panel). Since Iceland is located on the mid-Atlantic ridge where the lithospheric plates of Northern America and Eurasia drift apart, it is one of the regions on Earth most densely populated with volcanoes. In the right panel of fig. 10-6 the Katla volcanoe can also be detected by its faint degassing SO_2 plume.

Bromine Oxide – BrO

In recent years it has been discovered that in the polar troposphere ozone is often strongly depleted close to the surface in polar spring. Ozone destruction in the troposphere is catalysed by BrO in a similar way as in the stratosphere but here the source of bromine is natural, not anthropogenic. The details of the transfer of bromine from sea water to the atmosphere and the recycling on aerosols are not yet fully understood but satellite measurements from GOME and now SCIAMACHY (fig. 10-7, fig. 10-8) provide detailed maps of the BrO plumes that are producing these low ozone events. It is assumed that high salinity frost flowers (fig. 10-9) can develop quickly on the surface of the ocean under cold conditions. They contain bromide. When the sun is rising in the Arctic at the end of the winter the frost flowers vanish and release bromide into the atmosphere where it can be detected as BrO *(Kaleschke et al. 2004)*. Recent changes in sea ice coverage in the northern hemisphere raise the question if the pattern of ozone destruction is changing and through the link of bromine and mercury chemistry, this could have a substantial impact on the Arctic environment.

Formaldehyde – HCHO

For the formation of tropospheric ozone smog, both nitrogen oxides and volatile organic compounds (VOC) are needed. Therefore, SCIAMACHY's capability to also observe the short-lived HCHO – representing VOCs as well as indicating emissions of non-methane hydrocarbons – is relevant for pollution monitoring and the validation of atmospheric chemistry models.

HCHO is mainly produced from methane oxidation and hydrocarbon emissions (isoprenes, terpenes etc.) and has an average lifetime of a few hours, with the major sinks being photolysis and reaction with OH. The highest values occur above regions with evergreen broadleaf forests near to the equator due to the oxidation of biogenic VOC emissions. Other areas with enhanced values of formaldehyde are those with strong air pollution, e.g. the Red Basin in China, or with regular biomass burning, e.g. woodland and wooded grassland in Africa. These two contributions, anthropogenic and biogenic, can be clearly detected in HCHO maps derived from SCIAMACHY measurements (fig. 10-10).

Glyoxal – CHOCHO

Glyoxal is another representative of VOC and is known to be formed during the oxidation of a variety of biogenic emissions, e.g. isoprene, and of aromatic hydrocarbons. In contrast to formaldehyde, direct emissions of glyoxal are believed to be small and therefore it is a better indicator for VOC oxidation, the main source of photochemical smog. Its major sinks are photolysis and reaction with OH. The average lifetime of glyoxal is a few hours, which makes it challenging to be retrieved from satellite observation due to the absence of significant accumulation and transport into the free troposphere. Nevertheless, with data from SCIAMACHY it is now possible to get a first global picture of the glyoxal distribution (see fig. 10-11). Global observations of glyoxal, coupled with those of HCHO, identify photochemical hot spots in the Earth's atmosphere and constrain our understanding of biogenic emissions, biomass burning, and pollution.

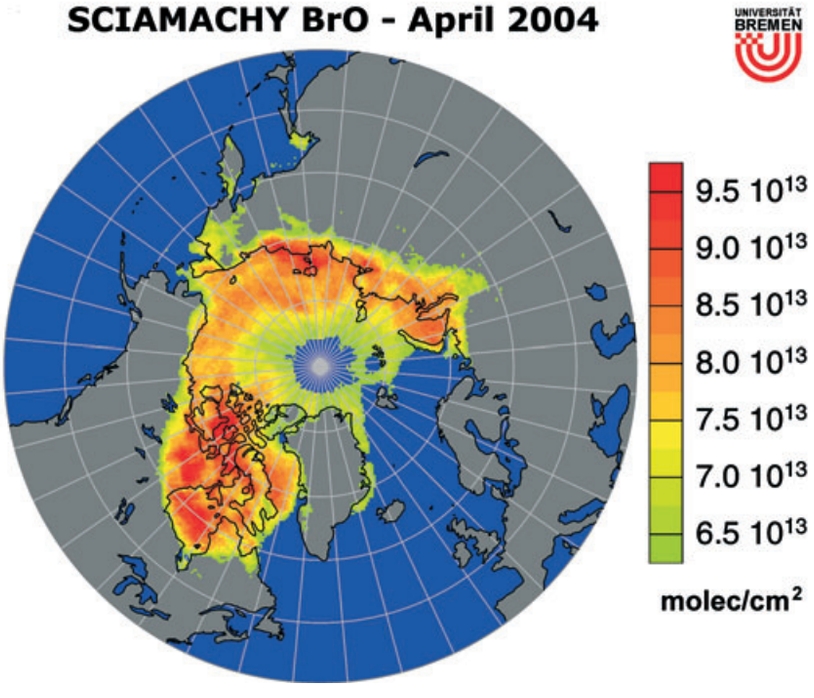

Fig. 10-7: BrO concentrations over the arctic sea ice in April 2004. (image: DLR-DFD and IUP-IFE, University of Bremen)

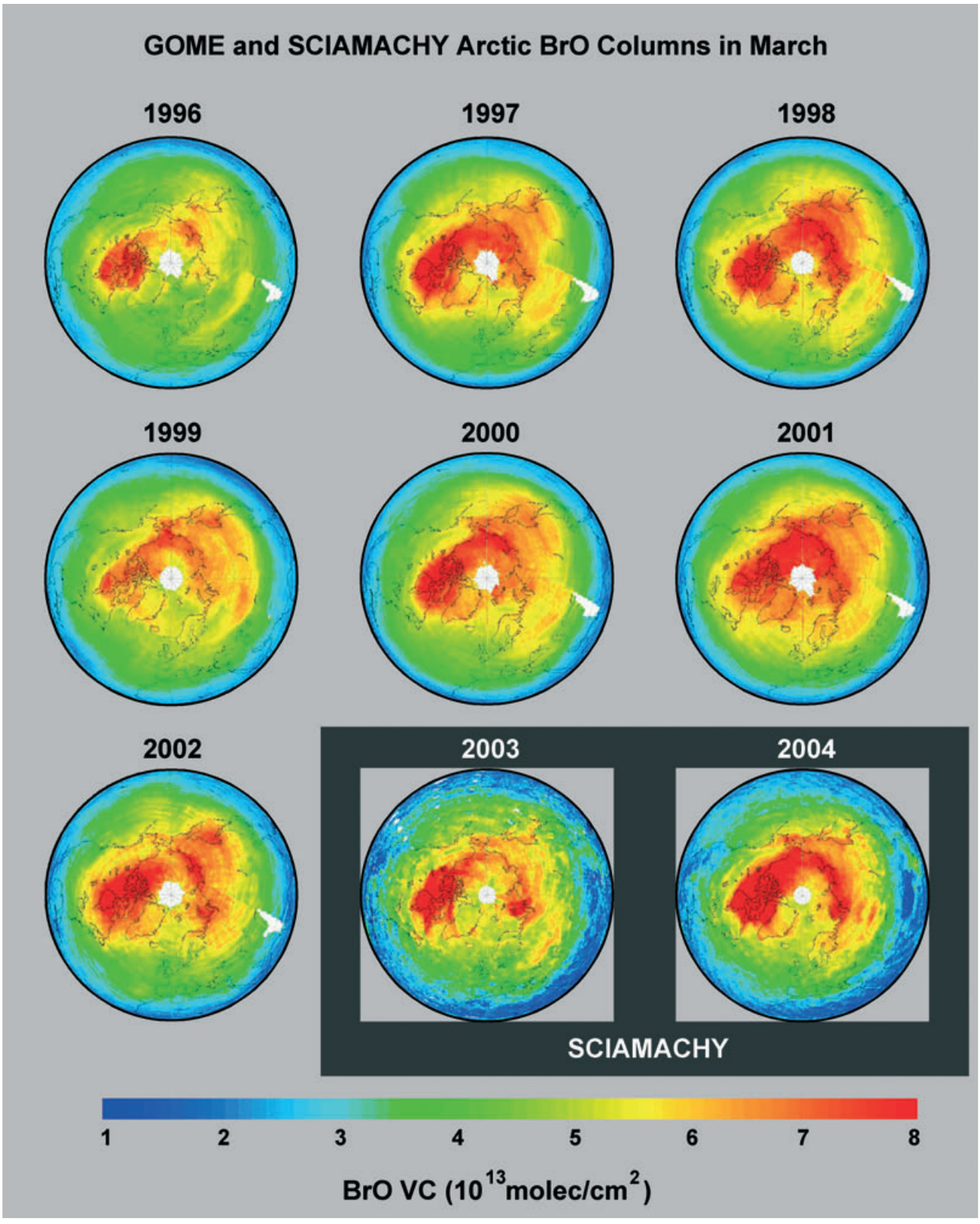

Fig. 10-8: A long-term study of BrO concentrations over the arctic ocean in March from 1996-2004 using data from GOME and SCIAMACHY. (images: M. Van Roozendael, BIRA)

Fig. 10-9: Frost flowers on the surface of water. They contain bromine which is released when the flowers begin to vanish at the end of the arctic winter. (photo: S. Kern, University of Hamburg)

Carbon Monoxide – CO

CO plays a central role in tropospheric chemistry as CO is the leading sink of the hydroxyl radical which itself largely determines the oxidising capacity of the troposphere. Therefore, it is of prime importance for the troposphere's self-cleansing efficiency and the concentration of greenhouse gases such as CH_4. CO also has a large air quality impact because it is a precursor of tropospheric ozone, a secondary pollutant which is associated with respiratory problems and decreased crop yields.

CO detection with SCIAMACHY is an ambitious task but current results show its feasibility. Carbon monoxide vertical columns can be retrieved from a number of CO absorption lines located around 2.3 μm in the SWIR range. The retrieval is not straightforward because these lines are relatively weak, much weaker than the absorption structures of the overlapping absorbers water vapour and methane and because of a number of calibration issues mainly related to large variable dark signals and a changing instrument characteristics as a result of the growth of an ice layer on the channel 8 detector (e.g. *Gloudemans et al. 2005*). Nevertheless, a first survey of global CO over land has been performed (fig. 10-12) which shows elevated CO in the case of fires due to biomass burning. These results are to a large degree consistent with MOPITT and model predictions *(de Laat et al. 2006)*.

Carbon Dioxide – CO_2

CO_2, the most important anthropogenic greenhouse gas, is regulated by the Kyoto Protocol and can be considered as a synonym for the impact of industrialisation on our environment. In pre-industrial times CO_2 mixing ratios dating back several thousands years were about 300 ppm at maximum. Present values are between 50-100 ppm higher, with the increase mainly attributed to the past 50 years as a clear indication of an anthropogenic effect. Carbon, dumped into natural sinks over millions of years, is now released into the atmosphere by fossil burning. In addition other anthropogenic activities such as deforestation reduces the ability of nature to recycle efficiently atmospheric CO_2. A thorough study of carbon dioxide is thus required to understand the global carbon cycle and to predict how greenhouse gases evolve with time. About 50% of the emitted CO_2 remains in the atmos-

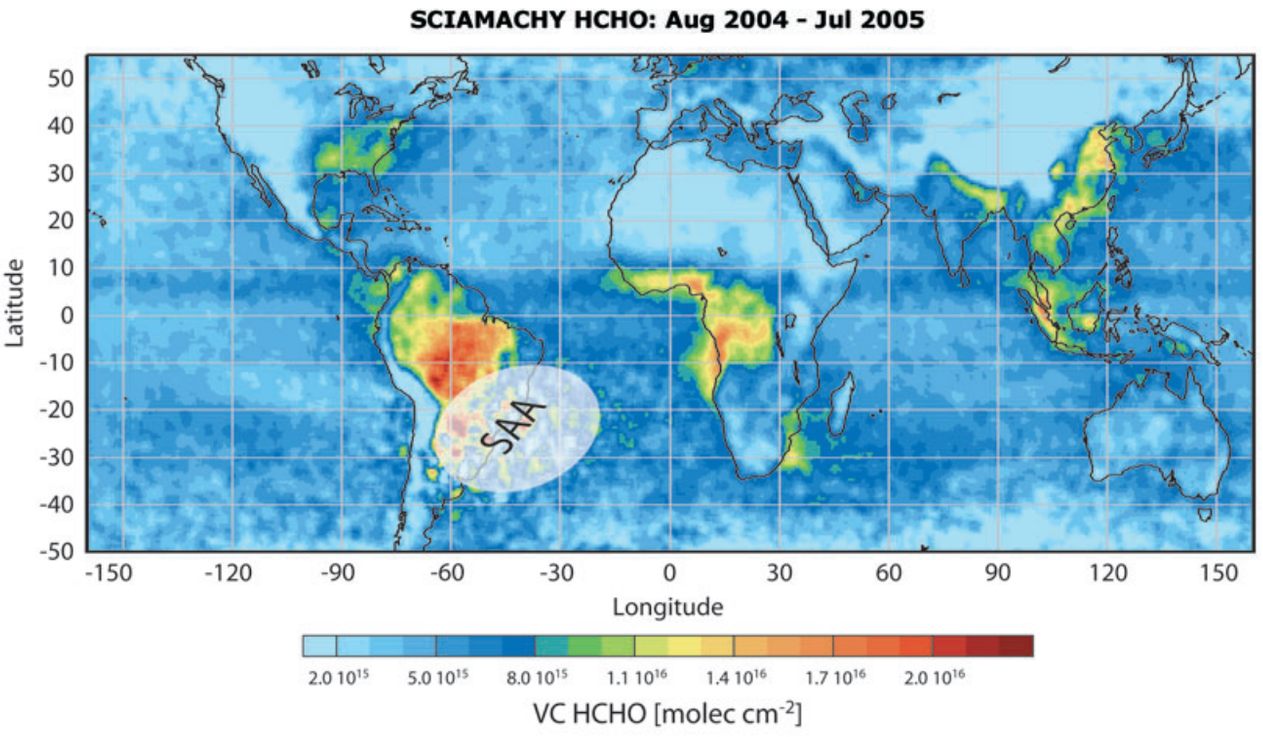

Fig. 10-10: The global distribution of formaldehyde (HCHO), derived from SCIAMACHY measurements from August 2004 to July 2005. In the SAA data analysis is of reduced quality. (image: F. Wittrock, IUP-IFE, University of Bremen)

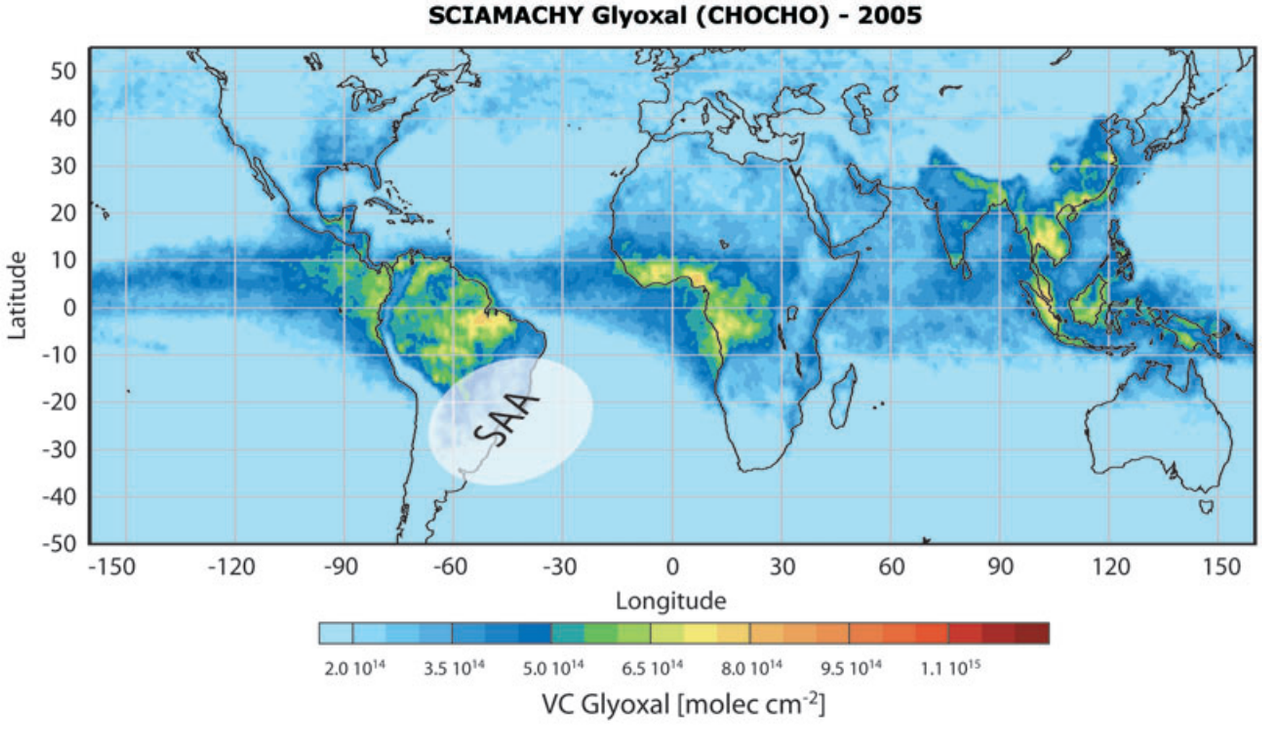

Fig. 10-11: The global distribution of glyoxal (CHOCHO) for the year 2005, as derived from SCIAMACHY measurements. In contrast to formaldehyde, direct emissions of glyoxal are believed to be small and therefore glyoxal is a better indicator for VOC oxidation, the main source of photochemical smog. In the SAA data analysis is of reduced quality. (image: F. Wittrock, IUP-IFE, University of Bremen)

phere, the other half is deposited in the oceans and in the biosphere. Photochemical processes in green leaves extract carbon dioxide from the troposphere over land. Thus large forest areas act as a CO_2 sink. The Siberian boreal forest in summer is one of these extended CO_2 sinks which can be observed by SCIAMACHY, as illustrated in fig. 10-13 displaying atmospheric CO_2 levels at various seasons over the northern hemisphere during the year 2003. SCIAMACHY nadir observations in the SWIR spectral region formed the basis for the retrieved CO_2 information *(Buchwitz et al. 2005, de Beek et al. 2006)*. The CO_2 mixing ratio has been obtained by normalising the CO_2 column with the simultaneously retrieved airmass from oxygen measurements.

Methane – CH_4

This species is considered to be the second most important anthropogenic greenhouse gas after carbon dioxide and is also regulated by the Kyoto Protocol. Compared to pre-industrial times methane concentrations have doubled due to anthropogenic emissions. A detailed knowledge of emission characteristics is required to better understand seasonal variations, the spatial distribution and the contribution from natural sources. Model calculations predict column averaged CH_4 volume mixing ratios. SCIAMACHY has obtained for the first time tropospheric methane densities and allows comparing models with actual global data.

The CH_4 retrieval quality is currently only reliable over land since low ocean reflectivity reduces the quality of the analysis over oceans. When accumulated over the period August-November 2003, the measured global methane densities *(Frankenberg et al. 2005)* show a pattern as displayed in fig. 10-14 (top). Prevailing winds seem to transport CH_4 over the oceans as indicated west of South America and Africa. A three-dimensional chemical transport model yields, for the same time, a methane distribution which is in general in good agreement with observations (fig. 10-14 bottom). Significant deviations do however exist in tropical rain forest areas. Here retrieved CH_4 columns are much higher than expected. The cause of these discrepancies still needs to be identified but independent retrieval algorithms show similarly elevated CH_4 densities in these regions *(Buchwitz et al. 2005)*. A likely cause of the discrepancy is the underestimation of methane emissions by plants, as recently pointed out by *Keppler et al. (2006)*. The newly identified CH_4 source in combination with the global CH_4 data set delivered by SCIAMACHY will have important implications for the global methane budget and

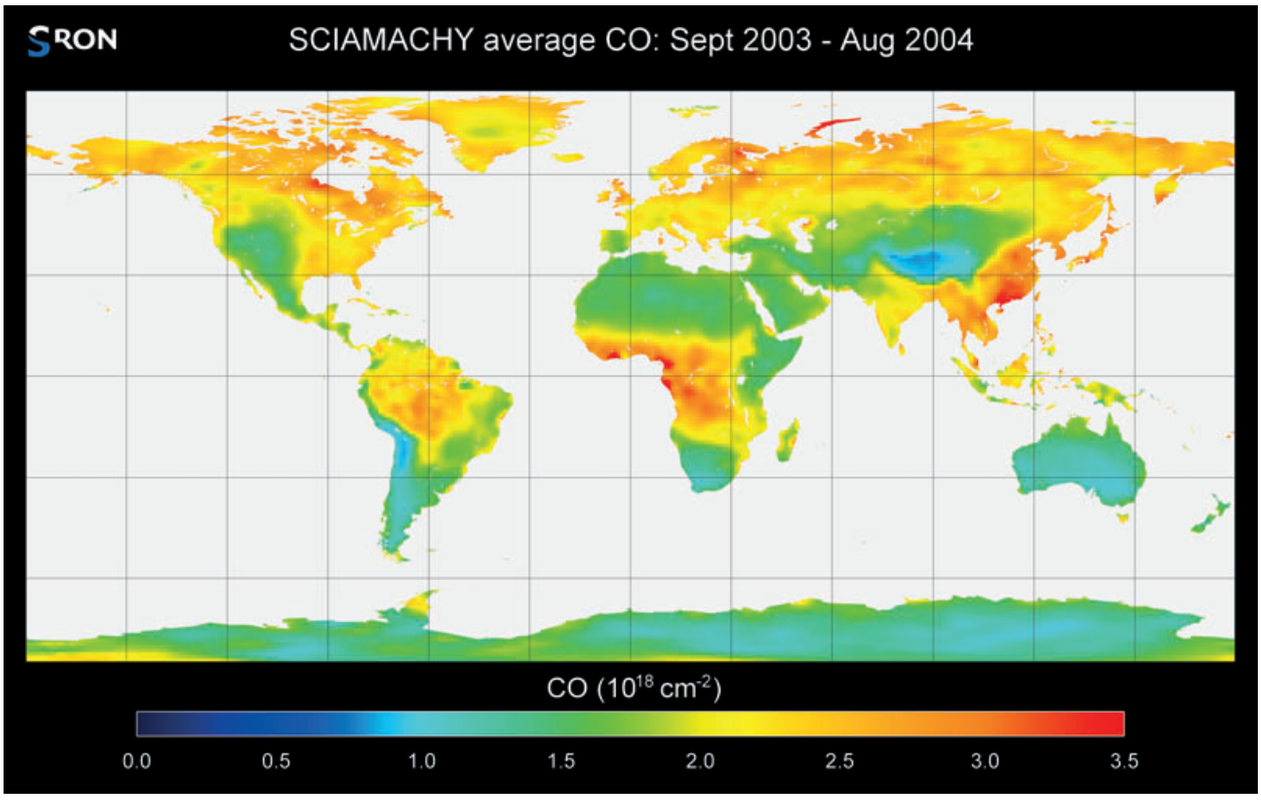

Fig. 10-12: The global distribution of carbon monoxide. Elevated CO is present in regions with biomass burning. The data is largely consistent with MOPITT and model results. (image: H. Schrijver, SRON)

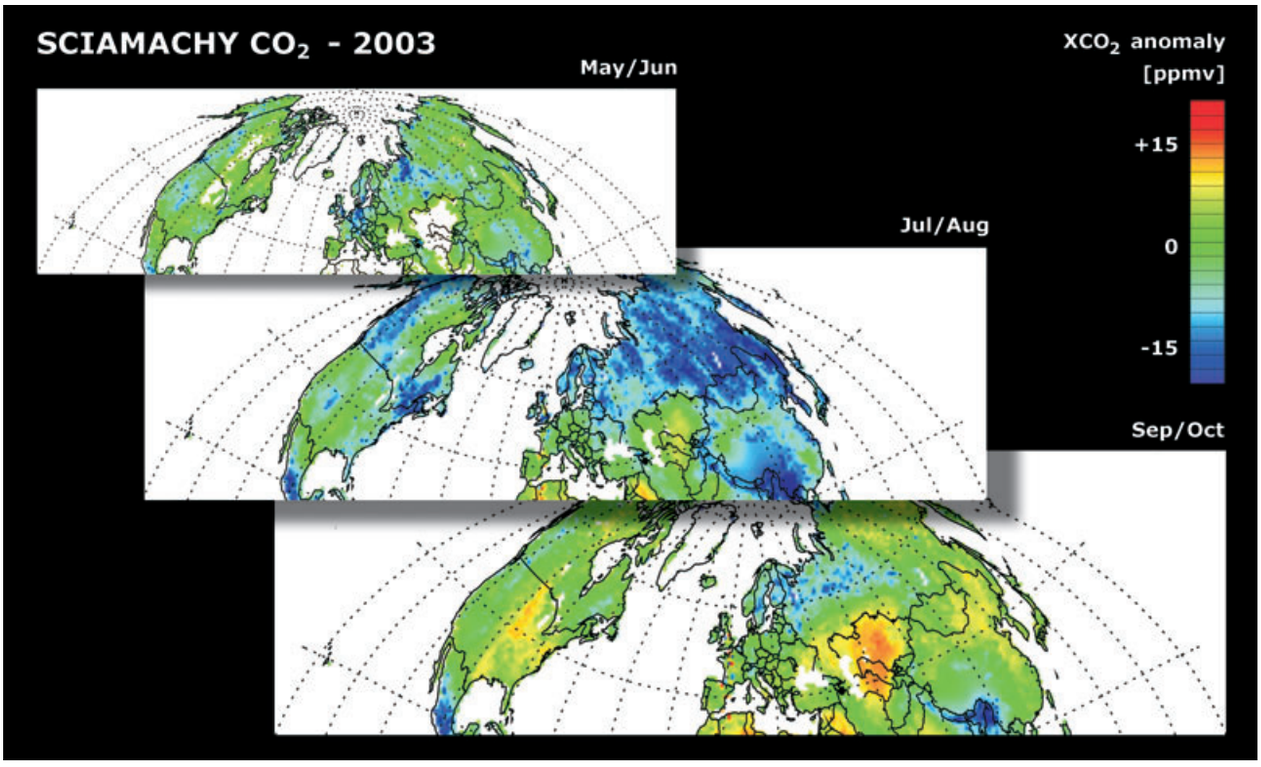

Fig. 10-13: Atmospheric CO_2 as measured by SCIAMACHY over the northern hemisphere during the year 2003. Low values (blue) during July/August compared to higher values (green and yellow) before and after this time period are due to uptake of atmospheric CO_2 by vegetation, e.g. boreal forests, which is in its growing phase during the summer months. (image: M. Buchwitz, IUP-IFE, University of Bremen)

will call for a reconsideration of the role of natural methane sources in past, present and future climate change.

Water Vapour – H_2O

Water vapour, the most important natural greenhouse gas, is a highly variable component of the atmosphere with direct anthropogenic impact on its levels being usually negligible. Its contribution may reach up to 4% of the atmospheric volume in the tropics and amounts to less than 1% in dry air conditions. Due to the relation between temperature and humidity, water vapour acts as a positive feedback to anthropogenic radiative forcing and is thereby indirectly affected by human activity.

In contrast to microwave instruments, SCIAMACHY water vapour data are available over both land and ocean down to the surface but only for at least partly cloud-free scenes (fig. 10-15). Because of their independence from other in-situ or remote sensing measurements, SCIAMACHY water vapour columns provide a new global data set *(Noël et al. 2004)*. A combination of SCIAMACHY water vapour results with corresponding data derived from GOME and follow-on instruments allows the study of water vapour long-term trends.

Aerosols

Due to their scattering and absorption effects, aerosols are a major element in the Earth's climate system. In addition, they impact on clouds and precipitation since they can act as cloud condensation nuclei thus affecting dramatically the optical properties of clouds. Aerosols occur in different types because they have different origins. Natural sources comprise volcanoes, dust storms, forest and grassland fires as well as sea spray. Anthropogenic activities, such as fossil fuel burning and changes of natural surface cover, also produce aerosols. These become an increasing concern in air quality issues. Averaged over the globe, aerosols made by human activities currently account for about 10 percent of the total amount of aerosols in our atmosphere. The complex properties of aerosol particles make it rather difficult to understand their roles in climate change, both on a regional and global scale. Even the question whether aerosols contribute to global warming or generate cooling, for example by modifying the terrestrial albedo, is not fully answered.

Aerosol measurements are not the primary focus of SCIAMACHY. Nevertheless, in comparison to other more aerosol specific sensors, it offers the opportunity to provide information about the absorp-

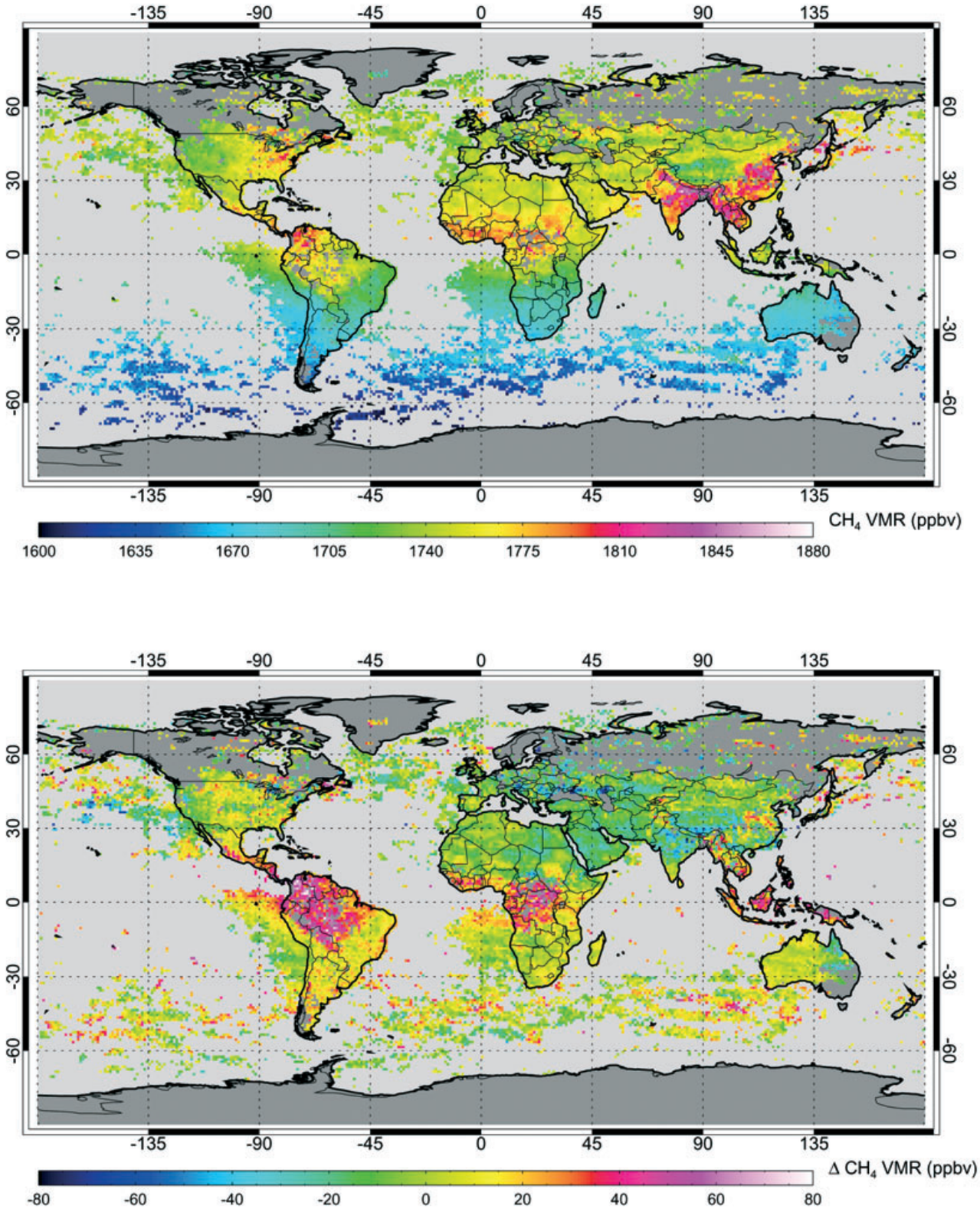

Fig. 10-14: Methane concentrations for August-November 2003 (top). Emissions are high in India and parts of China due to agricultural activities but also over tropical rainforests with still unknown reason. This phenomenon becomes obvious when measurements are compared with model calculations. In the bottom panel the difference between retrieved and modelled densities is shown with discrepancy 'hot spots' in Indonesia, Central Africa and South America. (images: *Frankenberg et al. 2005*)

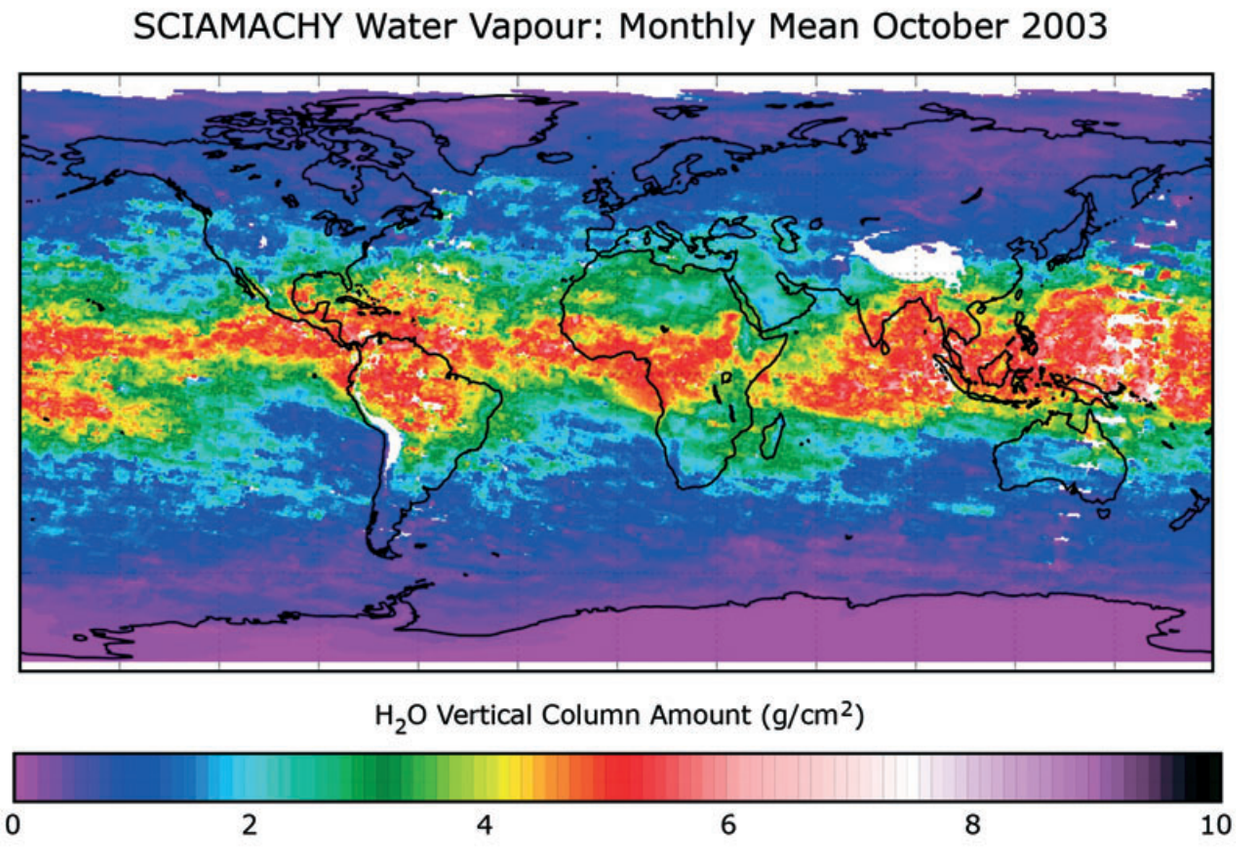

Fig. 10-15: Global monthly mean of gridded SCIAMACHY water vapour columns for October 2003. White areas denote either regions of missing SCIAMACHY data or high mountain areas where data have been removed by the inherent AMC-DOAS quality check. (image: S. Noël, IUP-IFE, University of Bremen)

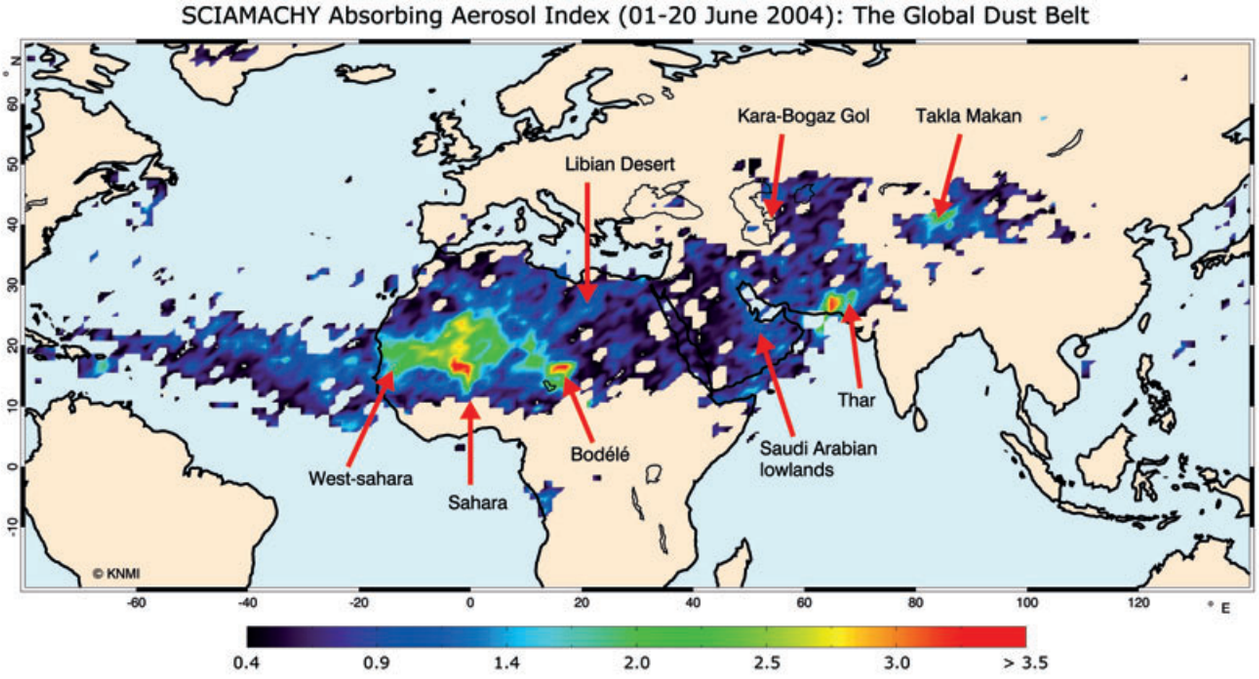

Fig. 10-16: The Global Dust Belt. A 20 day average of SCIAMACHY AAI in June 2004 shows the spatial distribution of desert dust, called the *Global Dust Belt (Prospero et al. 2002)*. Even from a 20 day average, AAI peaks coincide with the major desert areas in the northern hemisphere and the AAI shows Saharan dust being transported over the Atlantic Ocean. (image: M. de Graaf, KNMI)

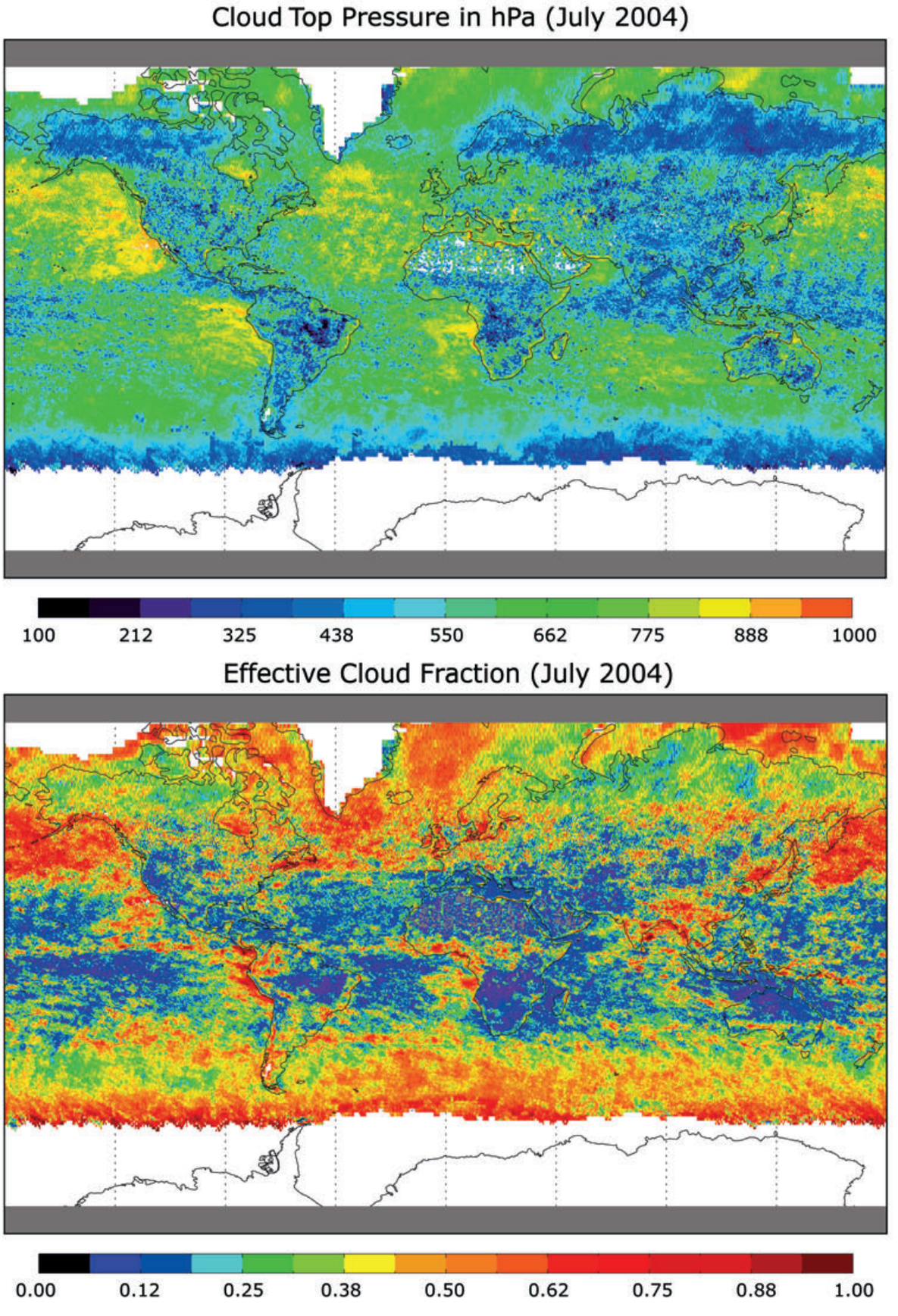

Fig. 10-17: Examples of global maps of SCIAMACHY O_2 A-band cloud results from the FRESCO algorithm: Effective cloud top pressure for July 2004 (top) and effective cloud fraction for July 2004 (bottom). (images: KNMI/ESA)

tive part of the interaction of the aerosol with the radiation field by measurements in the UV below 400 nm. One of the parameters describing the presence of UV-absorbing aerosol is the AAI. It is obtained over ocean and land where it predominantly indicates aerosols from desert dust or biomass burning particles. Fig. 10-16 displays a 20-day average of Absorbing Aerosol Index data for June 2004. The high AAI over North Africa and the Middle East can be attributed to dust plumes over desert areas thus forming Earth's 'global dust belt'. From the Western Sahara dust storms carry the aerosols far over the Atlantic. In Central Africa the AAI is a sign for massive biomass burning.

Clouds

Clouds play an important role in the Earth's climate system. The amount of radiation reflected by the Earth-atmosphere system into outer space depends not only on the cloud cover and the total amount of condensed water in the Earth's atmosphere but also on the size of droplets, the thermodynamic state of water in clouds, and vertical distributions of cloud parameters. The information about microphysical properties and spatial distributions of terrestrial clouds on a global scale can be obtained only with satellite remote sensing systems. The determination of cloud parameters from SCIAMACHY was demonstrated during the last years. *Kokhanovsky et al. (2005, 2006)* demonstrated the ability to determine cloud top height, cloud phase index, cloud optical thickness and cloud liquid water path for clouds with an optical thickness larger than 5. *Acarreta et al. (2004)* reported on the retrieval of the thermodynamic cloud phase while *Krijger et al. (2005)* presented first results on cloud/snow discrimination using SCIAMACHY PMD measurements. Finally *Fournier et al. (2006)* studied the improvement in effective cloud top height and cloud fraction (see fig. 10-17) determination over deserts, when the impact of the desert dust aerosol is properly taken into account in the surface albedo database.

10.2 Stratosphere

The stratosphere is the layer where public interest in the Earth's atmosphere has begun to grow with the detection of the ozone hole in the mid-1980's of the last century. During the last decades a steady decrease has been observed in the ozone abundance over the South Pole, North Pole and the mid latitudes of up to 3-6% per decade. The most striking feature is the massive loss of stratospheric ozone over Antarctica each southern spring. Ozone loss in the stratosphere over Antarctica at the end of the winter is so large because stratospheric temperatures drop to very low values in wintertime. Related to this phenomenon, the polar vortex develops which isolates the air during the polar night so that the cold conditions remain stable and Polar Stratospheric Clouds grow (see fig. 10-18). In this environment the chemistry of ozone depletion begins with the conversion of reservoir species to chemically active molecules on the surface of the PSCs. Finally, when the vortex breaks down in polar springtime, the PSCs disappear and release chemically active compounds. These react with ozone resulting in the destruction of the O_3 molecules. In addition, ozone loss was also observed in the tropics and mid-latitudes. Today there is broad agreement that in order to detect possible signs of recovery, a continuous monitoring of the ozone layer, the ozone hole and of those species impacting the ozone chemistry is required. In addition, the presence of PSCs needs to be understood as they can activate ozone depleting reservoirs.

SCIAMACHY allows exploitation of new opportunities using the limb backscatter as well as solar or lunar occultation measurement modes to determine vertically resolved concentration profiles of trace gases in the stratosphere, in addition to the column concentrations from the nadir measurement mode.

Ozone – O_3

The important role of ozone in the Earth's atmosphere can be attributed to the fact that it absorbs solar UV radiation which would otherwise reach the surface where it can cause damage to the biosphere. In the wavelength range below 290 nm, UV photons are almost completely blocked. Radiation from 290 nm to 320 nm is strongly attenuated so that dose levels on ground become no longer harmful. Ozone does not only impact conditions at the bottom of the troposphere but also in the upper atmosphere through the effects of absorption of UV to IR radiation and subsequent heating. The heating produces a temperature profile which makes the stratosphere vertically stable. Even transport mechanisms in the layers above – the mesosphere and thermosphere – were found to be influenced by the energy content of the stratosphere.

In the year of ENVISAT's launch the ozone hole over Antarctica differed significantly from what had been observed before. Its extent was reduced in 2002 by 40% as compared to previous years (fig. 10-19). However, this did not indicate a recovery of the ozone layer but originated from peculiar meteorological conditions where an unprecedented major stratospheric warming led to a split-up of the polar vortex which interrupted the heterogeneous processes leading

Fig. 10-18: Polar Stratospheric Clouds over Kiruna/Sweden. (photo: H. Berg, Forschungszentrum Karlsruhe, now with University of Toronto)

normally to the massive ozone destruction. A more detailed view of this September 2002 event was obtained by retrieving stratospheric profiles over Antarctica *(von Savigny et al. 2005a)*. The vertically resolved SCIAMACHY limb measurements showed that the ozone hole split did not occur throughout the entire stratosphere, but only above about 24 km. At 20 km there was still a single elongated area with low O_3 values (fig. 10-20). In normal cold Antarctic winters however, the O_3 profiles display a more regularly shaped ozone hole throughout the altitude range, as depicted for 2005 in fig. 10-20. The anomalous ozone hole from 2002 also developed quickly in time. Ozone losses computed from assimilated concentrations indicate that within a few days the situation changed drastically (fig. 10-21). This ozone hole split-up was already predicted in the 9 day ozone-forecast at KNMI (see *Eskes et al. 2005)*. The following years displayed again an ozone hole similar in size of those observed by SCIAMACHY's predecessor GOME (fig. 10-22).

Over the Arctic stratospheric temperatures are usually higher than over Antarctica, i.e. a stable polar vortex does not occur and PSCs are a much rarer phenomenon. Thus ozone depletion is not observed as a regular event in high northern latitudes at the end of the winter. However unexpected cold northern winters change the situation. This was the case in 2005 (e.g. *Bracher et al. 2005*). Measurements obtained with SCIAMACHY from January to March 2005 were compared with observations of 2004. A significant loss of ozone occurred over parts of Europe in February as a result of chlorine activation on PSCs when the sun rose after the long polar night. In March conditions had recovered and the O_3 levels approached their normal values (fig. 10-23).

Chlorine Dioxide – OClO

One key question related to the expected recovery of stratospheric ozone is the degree of chlorine activation observed in polar winter and spring in both hemi-

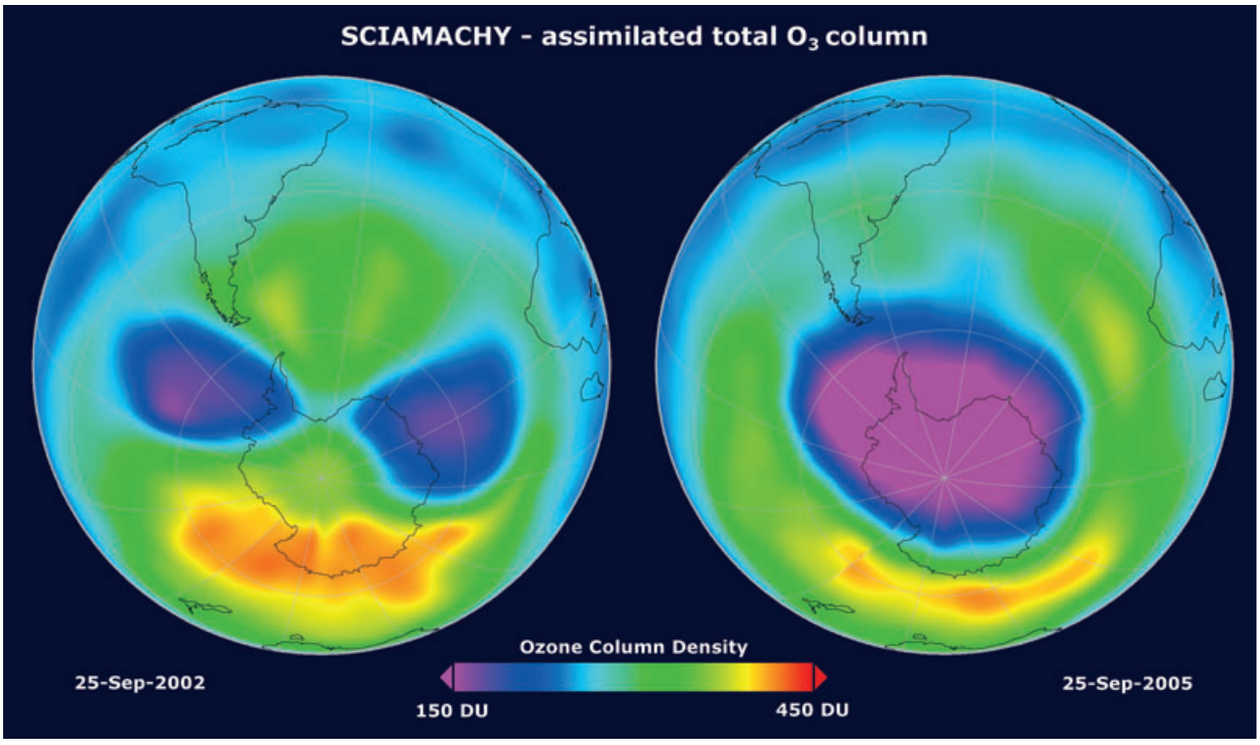

Fig. 10-19: The Antarctic ozone hole in 2002 (left) and 2005 (right). SCIAMACHY total column ozone measurements from September 25th have been analysed with the ROSE assimilation model to generate this view. Due to meteorological conditions the hole was split and reduced in size in 2002 but appeared 'as normal' in 2005. (images: T. Erbertseder, DLR-DFD)

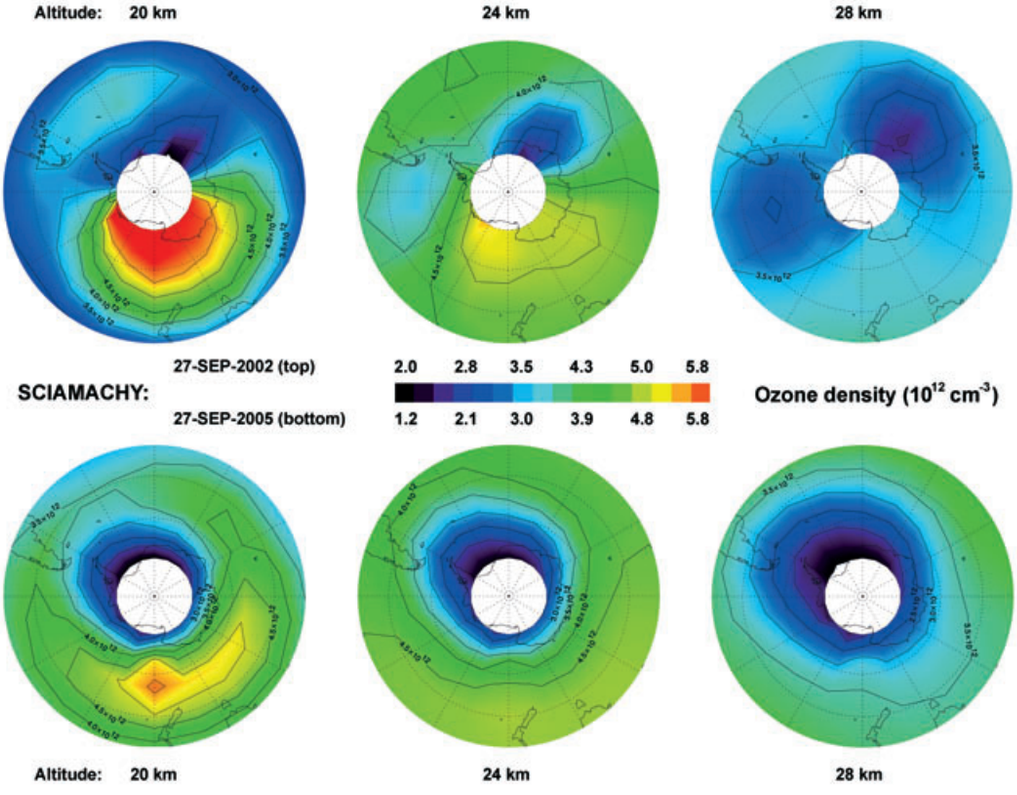

Fig. 10-20: Slices of the polar southern hemisphere ozone field at altitudes of approximately 20, 24 and 28 km on September 27th, 2002 and September 27th, 2005 as measured by SCIAMACHY. The observed split of the ozone hole in 2002 is not so obvious in the lower stratosphere around 20 km, but clearly visible at 24 and 28 km. In 2005 an ozone hole of 'normal shape' existed at all altitudes. (images: C. von Savigny, IUP-IFE, University of Bremen)

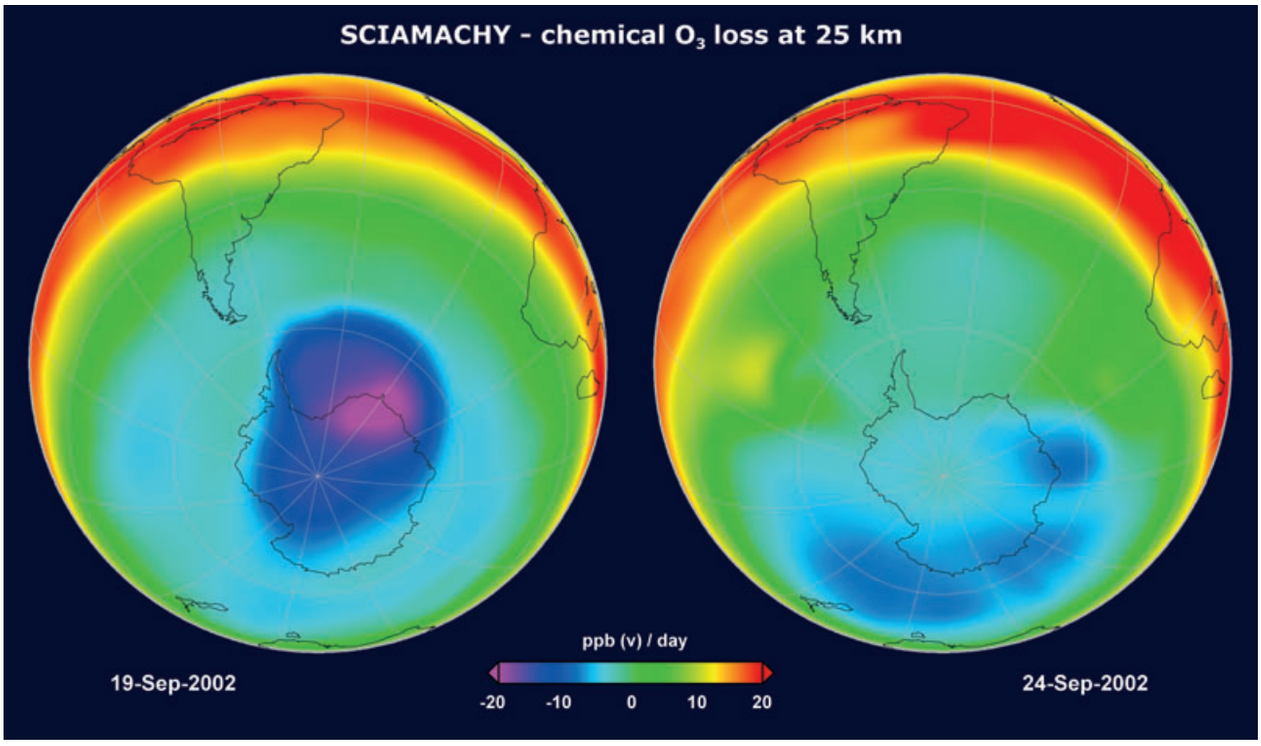

Fig. 10-21: Ozone losses on two days in September 2002 in the mid stratosphere at about 25 km, relative to the previous day. While on September 19th the ozone hole was still developing exhibiting its usual shape, 5 days later the split-up of the vortex has reduced ozone loss rates as compared to before. (images: T. Erbertseder, DFD-KA)

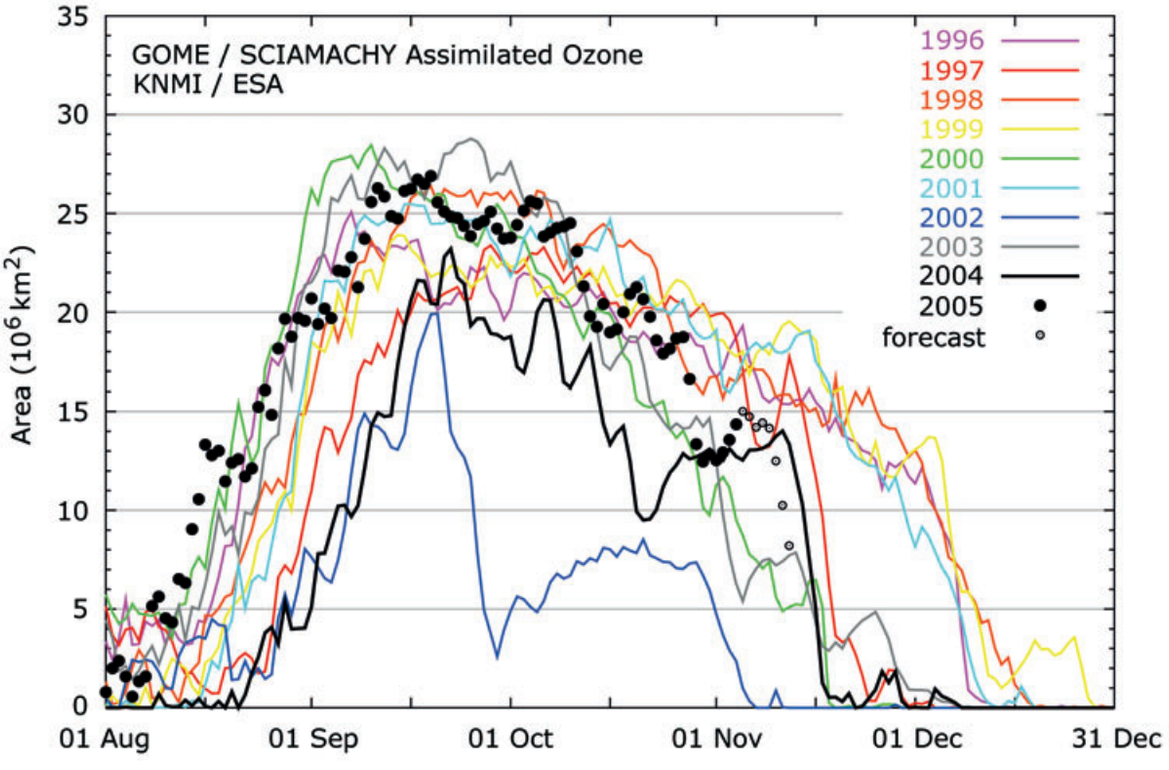

Fig. 10-22: Time series of the size of the Antarctic ozone hole from 1996-2005 based on observations of GOME and SCIAMACHY. The area includes ozone column values below 30° south lower than 220 Dobson Units. (graphics: KNMI/ESA)

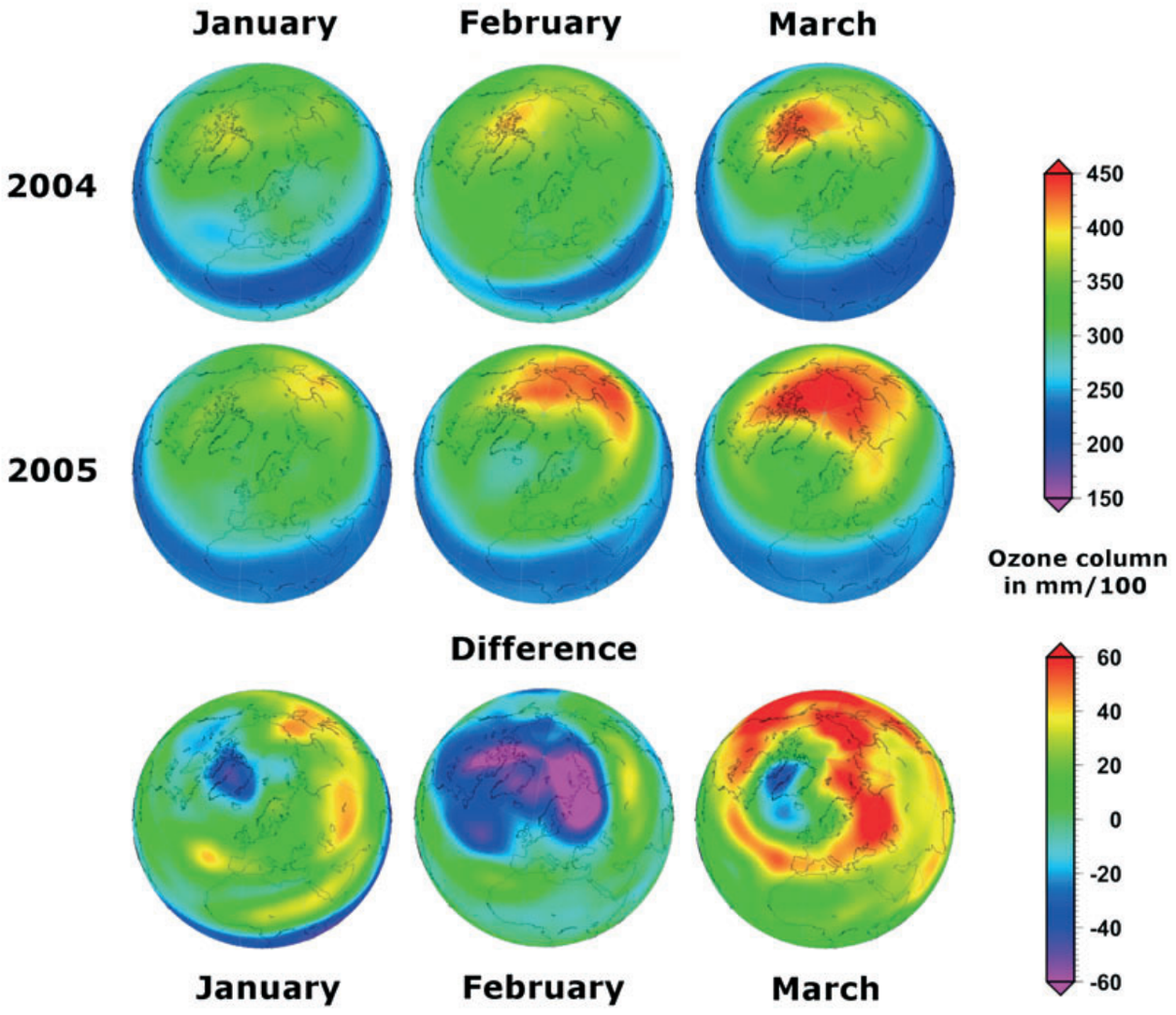

Fig. 10-23: Ozone columns over the northern hemisphere for late winter/early spring 2005 (mid row), 2004 (top row) and the difference between both years (bottom row). Caused by unusual low temperatures in the stratosphere over the Arctic, significant ozone loss occurred in February 2005 with a recovery of the ozone layer in March. (images: J. Meyer-Arnek, DLR-DFD)

spheres. This effect depends not only on the total available inorganic chlorine amount but also on the presence of PSCs for the activation of the chlorine reservoirs. The latter is a function of temperature and could change as the stratosphere cools in response to increased concentrations of greenhouse gases. One good indicator for chlorine activation is the presence of OClO which is formed by reaction of BrO and ClO. As stratospheric BrO concentrations are relatively constant, the OClO column is proportional to ClO concentrations. Time series of OClO were started with GOME and continued from 2003 onwards with SCIAMACHY data. Fig 10-24 displays for the southern hemisphere how OClO increases in the polar winter and decreases when spring begins. The peak corresponds to the maximum of the ozone hole.

Sometimes chemically active chlorine can also be observed in the boreal (northern) hemisphere. Under very cold conditions, as it was for example the case in winter 2004/2005, large amounts of these compounds are produced. SCIAMACHY monitored the north-polar region from 2003-2005 and detected highly variable chlorine concentrations (fig. 10-25). The moderate winter in 2003 resulted in small amounts of active chlorine, while 2004 was a very mild winter and no molecules could be detected. Early in 2005 however, the long and cold winter was well suited for the generation of active chlorine which finally caused a northern ozone hole.

Bromine Oxide – BrO

Bromine compounds play an important role in the catalytic destruction of stratospheric ozone. Despite their importance, however, there are only few measure-

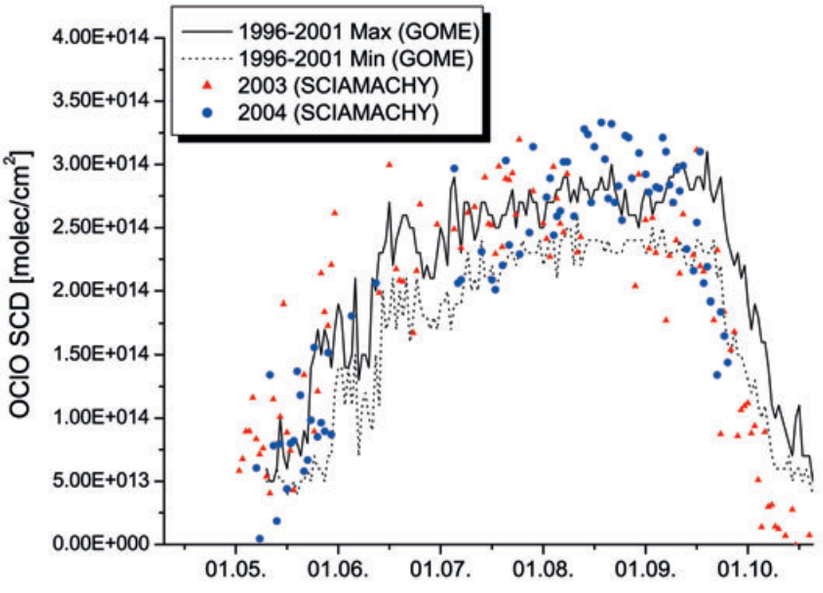

Fig. 10-24: OClO densities in the stratosphere of the southern hemisphere since 1996. SCIAMACHY retrievals fit well to the GOME time series. High OClO values coincide with the ozone hole season. (graphics: *Kühl et al. 2006*)

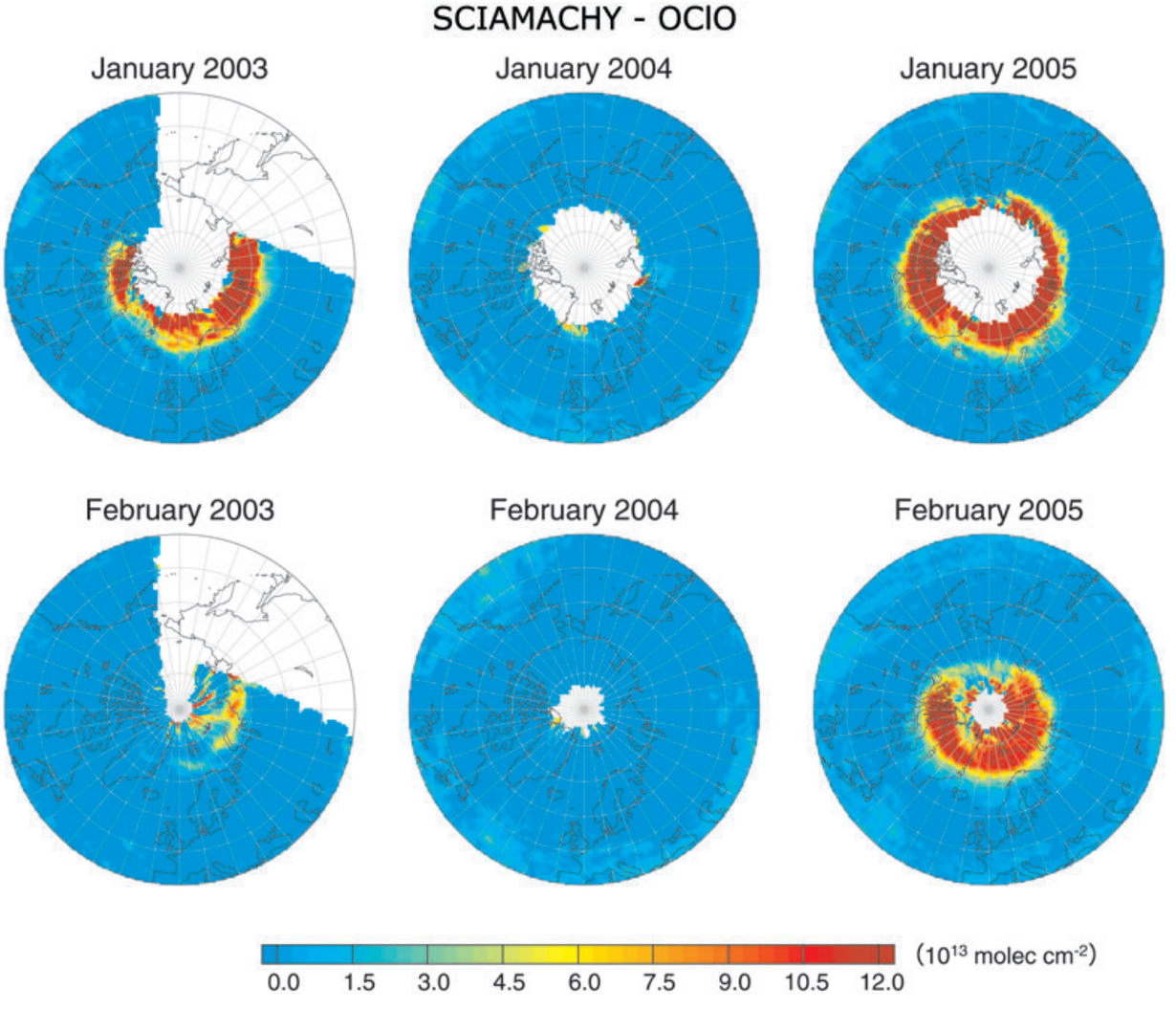

Fig. 10-25: Chemically active chlorine concentrations in the northern hemisphere in winter 2003-2005. Mild winters produce small, very cold winters – like 2005 – very large amounts of chlorine as depicted by the red areas in the 2005 OCIO maps. (images: A. Richter, IUP-IFE, University of Bremen)

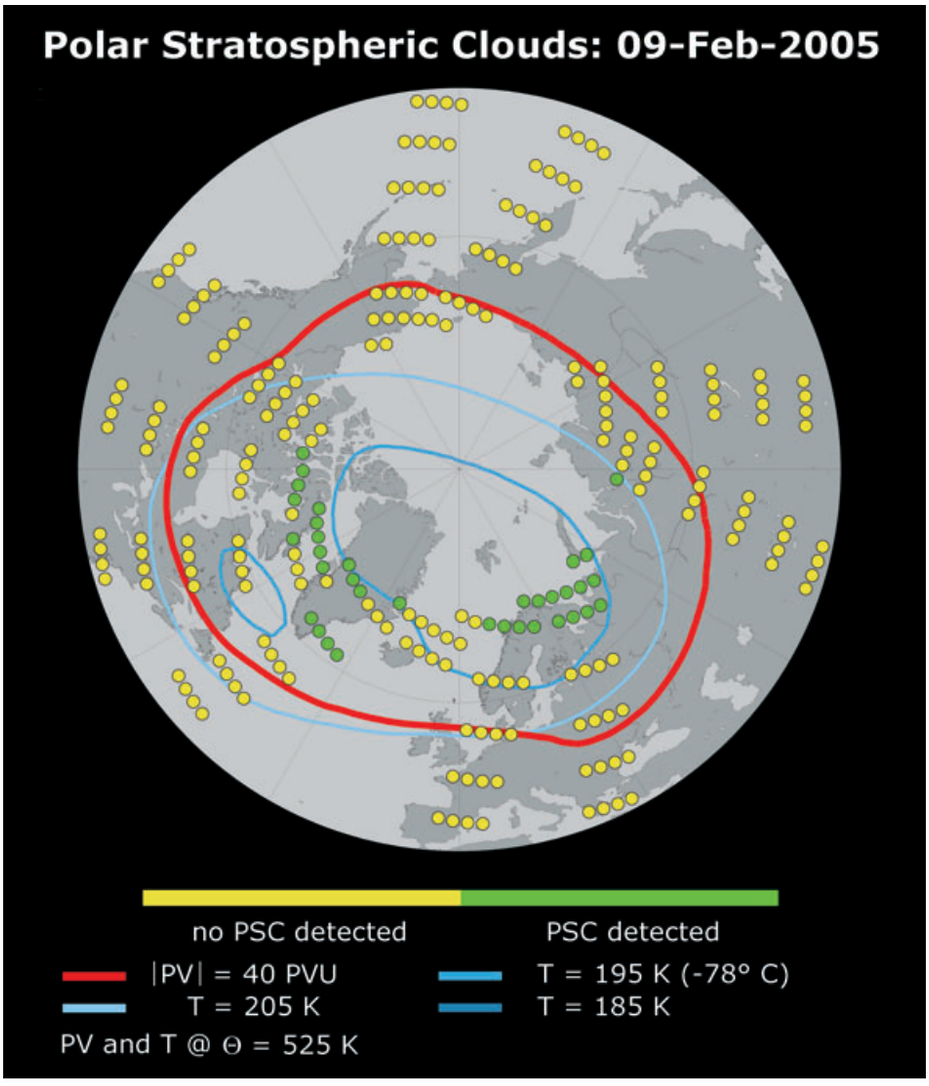

Fig. 10-26: Northern hemisphere map of PSCs for February 9th, 2005. The circles indicate the locations of limb measurements with green circles corresponding to detected PSCs. They are superimposed to the UK MetOffice temperature field at 525 K potential temperature, i.e. an altitude of about 22 km, and agree well with the temperature threshold for their formation. The temperature of 185 K was not reached on February 9th, 2005. (image: C. von Savigny/K.U. Eichmann IUP-IFE, University of Bremen)

ments of bromine compounds in the stratosphere. For the first time, SCIAMACHY provides global observations of stratospheric BrO profiles down to the lower stratosphere *(Sinnhuber et al. 2005)* thus permitting the understanding and validation of our current knowledge of the bromine chemistry and budget.

Polar Stratospheric Clouds – PSC

As already mentioned above, PSCs play a key role in the chemical processes which lead to severe ozone depletion in the stratosphere. These clouds are necessary to transfer inactive chlorine compound reservoirs such as HCl and $ClONO_2$ to active Cl that participates in different catalytic O_3 destruction cycles. They form at altitudes of about 15-25 km and exist as different types: Type Ia consists of crystalline NAT (nitric acid tri-hydrate) particles, the liquid type Ib PSCs consist of ternary solutions of nitric acid, sulphuric acid and water. Type II PSCs are made of water ice.

A common feature of all types is that they only form at very low temperatures of less than about -78°C (195 K). PSCs scatter solar radiation and thus affect the measured limb radiance spectra. Since PSCs are Mie-scatterers in the UV-SWIR spectral range, the spectral dependence – although highly variable – of their scattering cross section differs from the λ^{-4} spectral dependence of the molecular Rayleigh scatterers. This spectral difference can be exploited in a colour-index approach to detect PSCs (*von Savigny et al. 2005b*). How SCIAMACHY limb measurements are used to map PSCs is shown in fig. 10-26. In most cases there is a good correspondence between the detected PSCs and their formation threshold of -78°C.

10.3 Mesosphere

The density in the mesosphere is very low as 99% of the mass of the atmosphere can be found below 40 km. Because absorption of solar UV photons occurs in the layer below, the stratosphere, energy

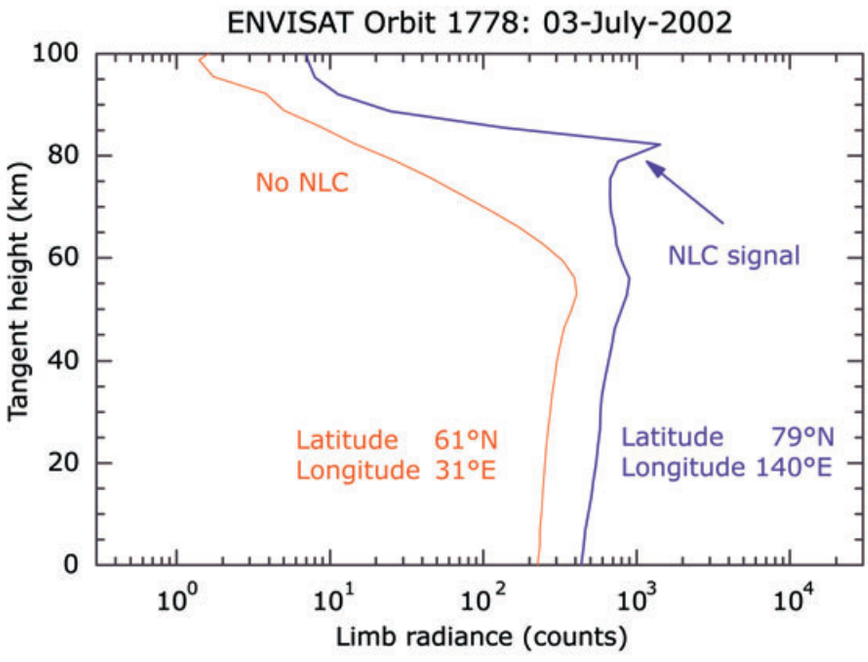

Fig. 10-27: NLC signature in UV limb radiance profiles. The scattering by ice particels in the NLC leads to a significant increase of the observed limb radiance profiles peaking at the characteristic NLC altitude of about 83-85 km (blue line). Shown in red is for comparison a limb radiance measurement without NLCs being present. (graphics: C. von Savigny, IUP-IFE, University of Bremen)

input to the mesosphere is limited to solar energy deposited into the mesosphere by O_2 absorption in the Schumann-Runge continuum bands between 100 and 200 nm. Temperatures in the mesosphere decrease again with increasing altitude. At the base of the mesosphere around approx. 50 km the temperature is about 0°C, while at the top, around 80 km, usually the lowest temperatures in the Earth's atmosphere can be found with -95°C, but extreme values can reach up to -160° C at the polar summer mesopause. Chemically, the mesosphere is characterised by a rather constant mixture of gases with nitrogen, oxygen, argon and carbon dioxide being the most abundant species.

Noctilucent Clouds – NLC

Noctilucent clouds, sometimes also referred to as *Polar Mesospheric Clouds*, are a high latitude summertime mesospheric phenomenon, even observable from ground. They occur at altitudes of about 83-85 km near the polar summer mesopause and consist of H_2O ice particles with radii ranging from a few nm up to about 80-100 nm. NLCs received a significant amount of scientific interest in recent years, since they may be early indicators of global change. The scattering properties of the NLC particles allow mapping of these high altitude clouds. Since they scatter solar radiation efficiently, they can affect the measured limb radiance profiles significantly, particularly in the northern hemisphere where scattering angles at polar latitudes are particularly small for SCIAMACHY limb observations. The NLC component of the measured limb signal, the blue curve in fig. 10-27, can be 2 orders of magnitude larger than the Rayleigh signal (red curve in fig. 10-27) at the NLC altitude, allowing for a simple detection of NLCs.

Apart from the detection and mapping of NLCs, SCIAMACHY observations also permit the estimation of the NLC particle size (see fig. 10-28). For wavelengths below about 310 nm, the multiple scattering and surface reflection components to the limb signal are negligible. In the resulting single scattering approximation, the spectral exponent of the NLC scattering spectrum can be related to the NLC particle size assuming for example Mie theory and the refractive index of H_2O ice *(von Savigny et al. 2004a)*.

Mesospheric Emissions

A number of atomic and molecular emission signals from the mesosphere and lower thermosphere are visible throughout the SCIAMACHY spectral range, e.g., OH Meinel band emissions (see below), the sodium lines, and several transitions from excited-state O_2. Of special interest is the UV wavelength range. Here, emissions from the NO gamma bands and a number of metallic species – e.g. iron and magnesium – can be observed as well as their ions, Fe+ and Mg+ (fig. 10-29). Additionally, a number of non-metallic species have been detected, namely atomic oxygen and silicon.

From the NO gamma band emissions, distributions of NO at 92 km are derived. NO is produced in the thermosphere and upper mesosphere by ionisation processes related to the aurora and transported downward into the mesosphere and stratosphere during polar winter. NO number densities in the altitude

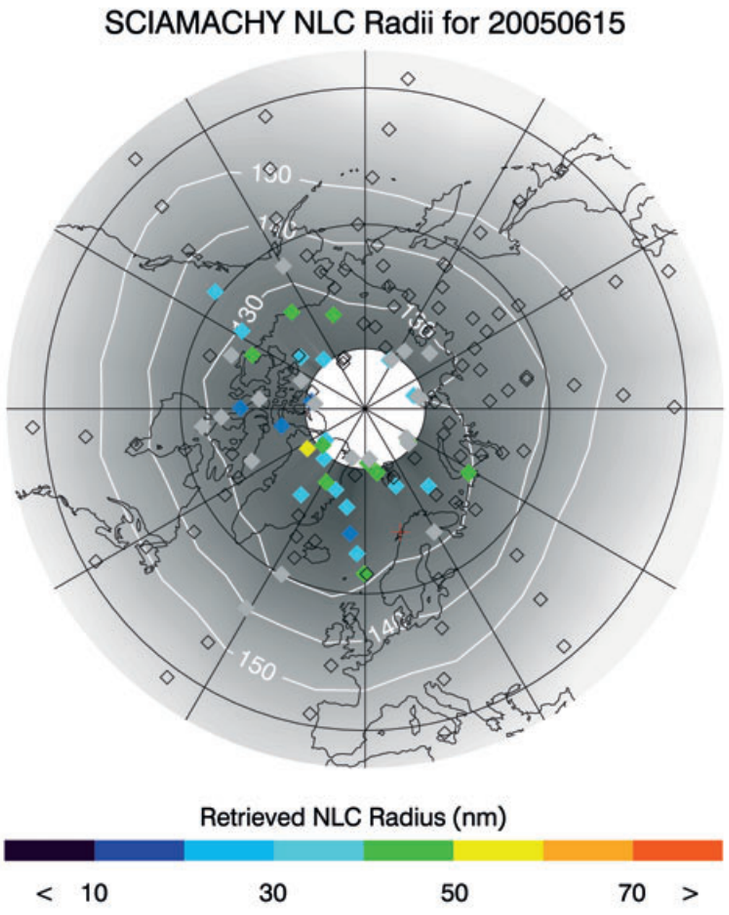

Fig. 10-28: NLC particle sizes for June 15th, 2005 derived from SCIAMACHY limb measurements. The grey solid diamonds indicate thin – but detectable – NLCs that did not allow a reliable size determination. The white contours indicate the temperature field at 83 km altitude as measured with AURA/MLS. (image: C. von Savigny, IUP-IFE, University of Bremen)

range of 70 km up to 92 km can be retrieved. The first results for January 2004 (fig. 10-30) show a tight correlation of NO with the aurora zone. In the northern winter hemisphere, NO is rather more long-lived than in the southern summer hemisphere, and consequently, NO values are higher there.

OH* Rotational Temperatures

SCIAMACHY permits for the first time the retrieval of OH* rotational temperatures at the mesopause from satellite measurements. OH* is vibrationally excited at the mesopause through the reaction of H and O_3. This produces an OH* emission layer centered at about 87 km with a width of 8-10 km. Several of the OH* Meinel emission bands are observable in the SCIAMACHY spectral range, e.g., the OH* (3-1) band at around 1500 nm as shown in the inset of fig. 10-31. This emission band is used for the retrieval of OH* rotational temperatures because it is one of the most intense Meinel emission bands. From the relative intensity of two or more rotational lines the effective temperature of the emitting layer can be retrieved from SCIAMACHY data (see fig. 10-31). This method has been applied for several decades to retrieve mesopause OH* rotational temperatures from ground measurements (e.g. *Bittner et al. 2002*). Therefore, coincident ground-based OH* rotational temperature measurements over Wuppertal and Hohenpeissenberg (Germany) as well as Hawaii *(von Savigny et al. 2004b)* could be used to validate the novel SCIAMACHY space-based approach. A comparison of both methods showed very good agreement.

Mesospheric Ozone and the October/ November 2003 Solar Storm

Highly energetic protons ejected from the sun during phases of high coronal activity reach the Earth with the solar wind and ionise the atmosphere and subsequentially lead to the formation of HO_x and NO_x. Both families participate in catalytic O_3 destruction cycles, with HO_x being more efficient above about 50 km and NO_x below about 50 km. Consequently enhanced O_3 destruction is expected after a strong solar proton event (SPE). A good opportunity to study the impact of solar activity on mesospheric ozone fields was a period in October/November 2003 – also known as 'Halloween Sun Storm' – when the sun exhibited extremely large coronal SPEs. Fig. 10-32 presents an analysis of the impact of the solar proton event at the end of October 2003 on the upper atmospheric O_3 *(Rohen et al. 2005)*. A strong ozone depletion of more than 50% even deep in the stratosphere is observed at

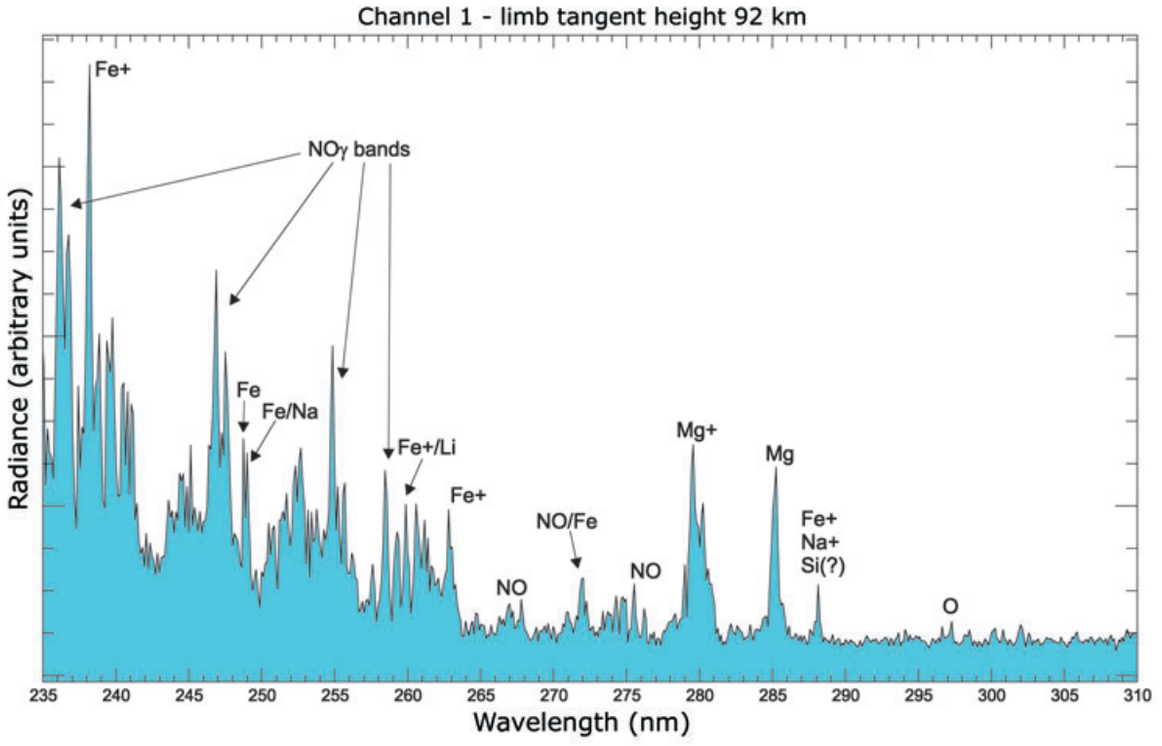

Fig. 10-29: Emission lines in SCIAMACHY limb radiance in channel 1 at the highest tangent altitude of about 92 km, normalised to the solar irradiance, in arbitrary units. A number of emission signals is detected here; the most dominant features are the NO gamma-bands and MgII, but signals from neutral Mg, atomic oxygen, Si, Fe and Fe+ are observed as well. (graphics: M. Scharringhausen, IUP-IFE, University of Bremen)

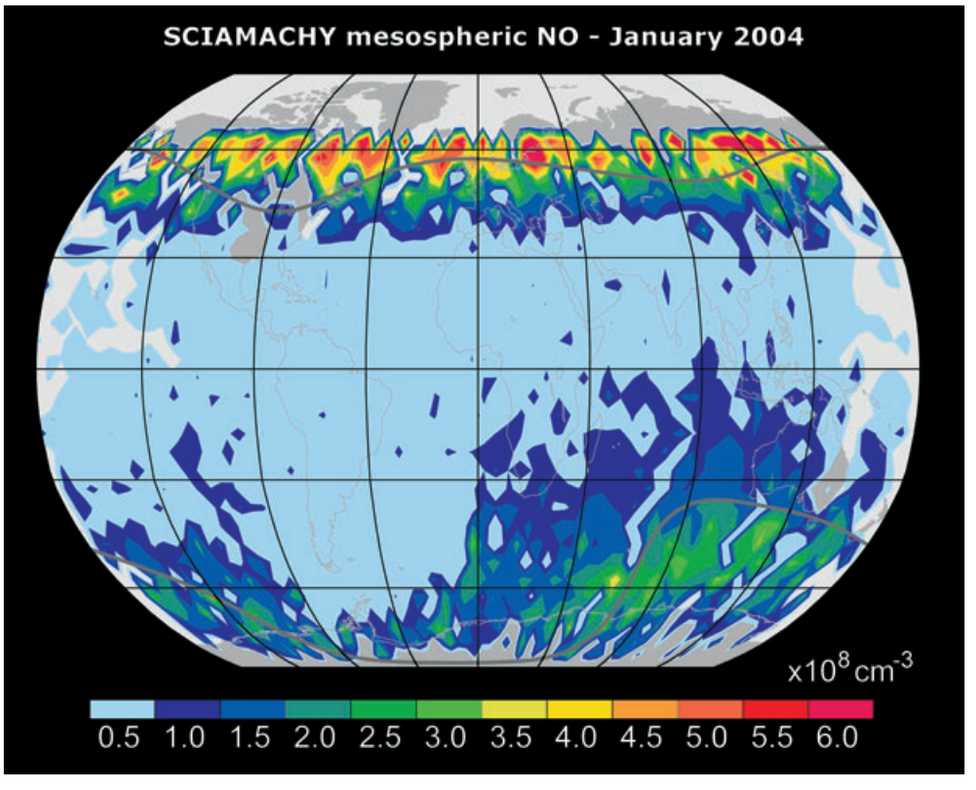

Fig. 10-30: Global distribution of NO number densities at 92 km altitude, averaged over a 5° grid, monthly average of January 2004. The dark grey lines denote 55° of geomagnetic latitude, i.e. the outer edge of the auroral oval. Over South America and the South Atlantic the high particle fluxes in the SAA prevent data retrieval and cause a data gap. No data are available north of 65°, as this area is in polar night. (image: M. Sinnhuber/M. Scharringhausen, IUP-IFE, University of Bremen)

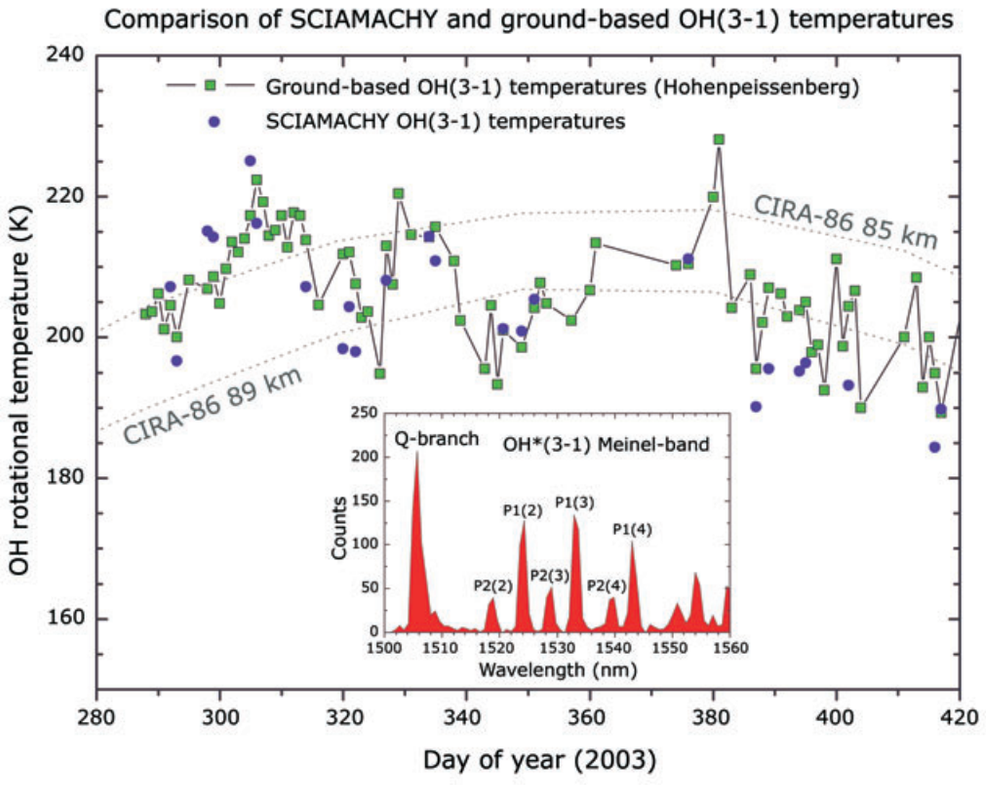

Fig. 10-31: Variation of the temperature at the mesopause derived from SCIAMACHY nighttime limb emission spectra (inset) in the OH-Meinel bands at a tangent height of 85.5 km. The inset shows the Q-branch (at 1507 nm) and the P-branch rotational lines of the OH^* (3-1) vibrational transition. (image: C. von Savigny, IUP-IFE, University of Bremen with ground based measurements kindly provided by M. Bittner and D. Offermann)

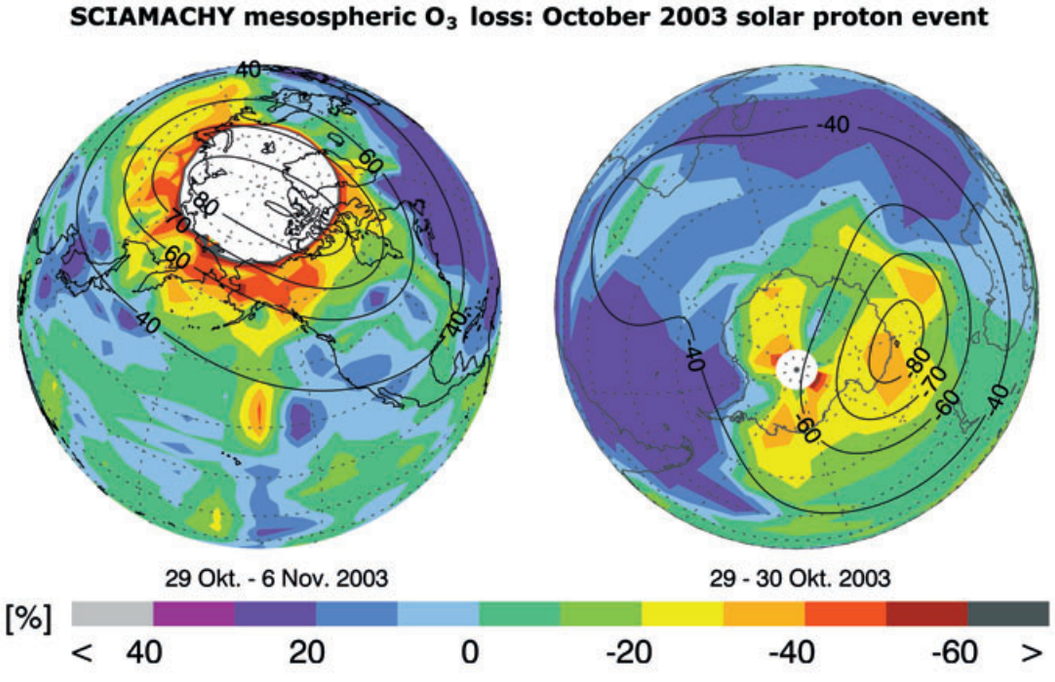

Fig. 10-32: Measured change of ozone concentration at 49 km altitude due to the strong solar proton events end of October 2003 in the northern and southern hemisphere relative to the reference period of October 20-24, 2003. White areas depict regions with no observations. The black solid lines are the Earth's magnetic latitudes at 60 km altitude for 2003. (image: *Rohen et al. 2005*)

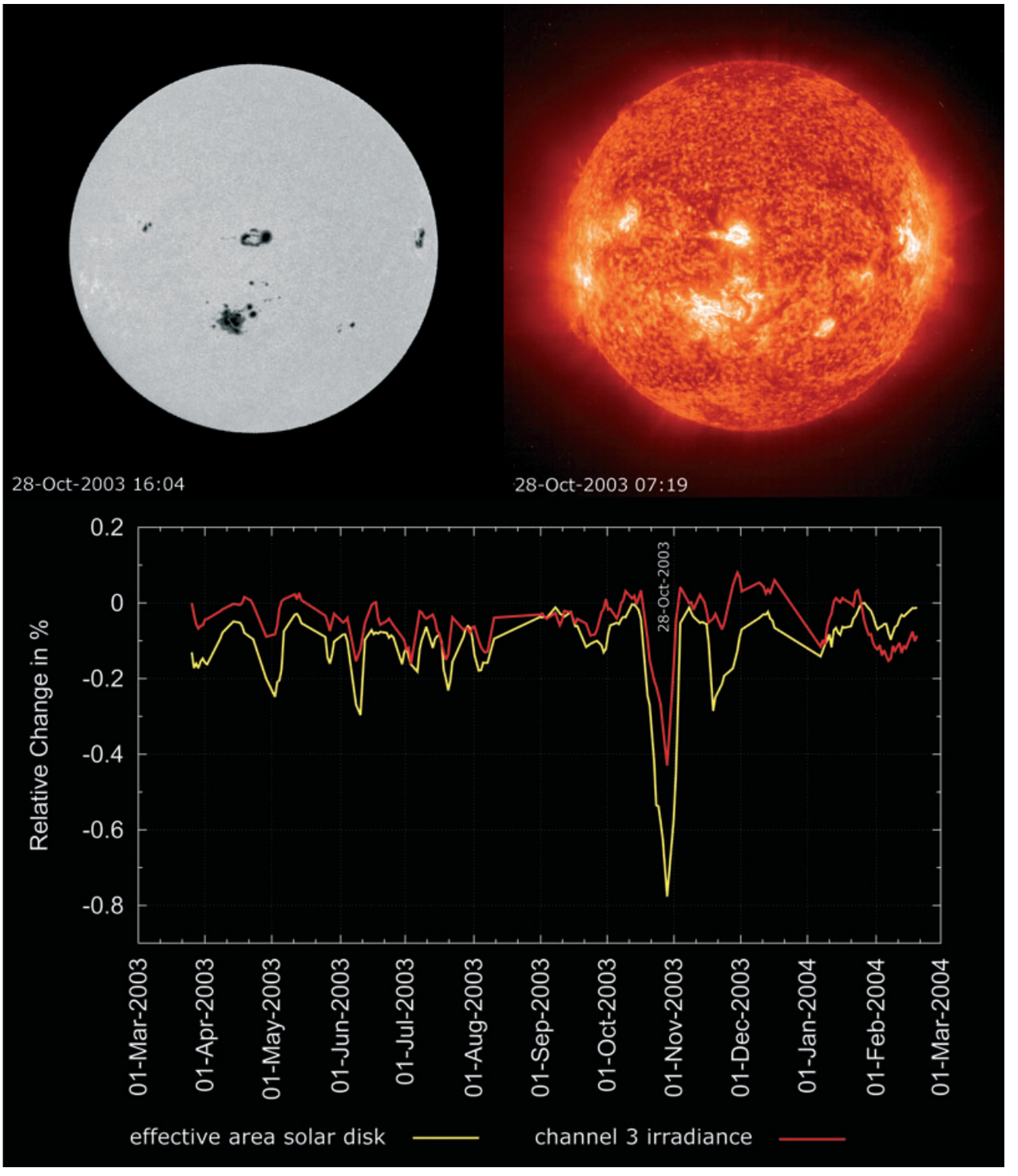

Fig. 10-33: The active sun on October 28th, 2003, in white light (top left), EUV at 304 Å (top right) and the signal in channel 3 as measured by SCIAMACHY. (images: Big Bear Solar Observatory, SOHO and IUP-IFE, University of Bremen)

high geomagnetic latitudes in the northern hemisphere, whereas the observed ozone depletion in the more sunlit southern hemisphere is much weaker. The mesospheric O_3 retrieval scheme *(Rohen et al. 2006)* is based on the same principles as the stratospheric O_3 retrieval but using the spectroscopic information from the O_3 Hartley band in the UV. SCIAMACHY measurements of the O_3 loss agree well with model simulations, indicating that the main processes leading to the O_3 loss are fairly well understood.

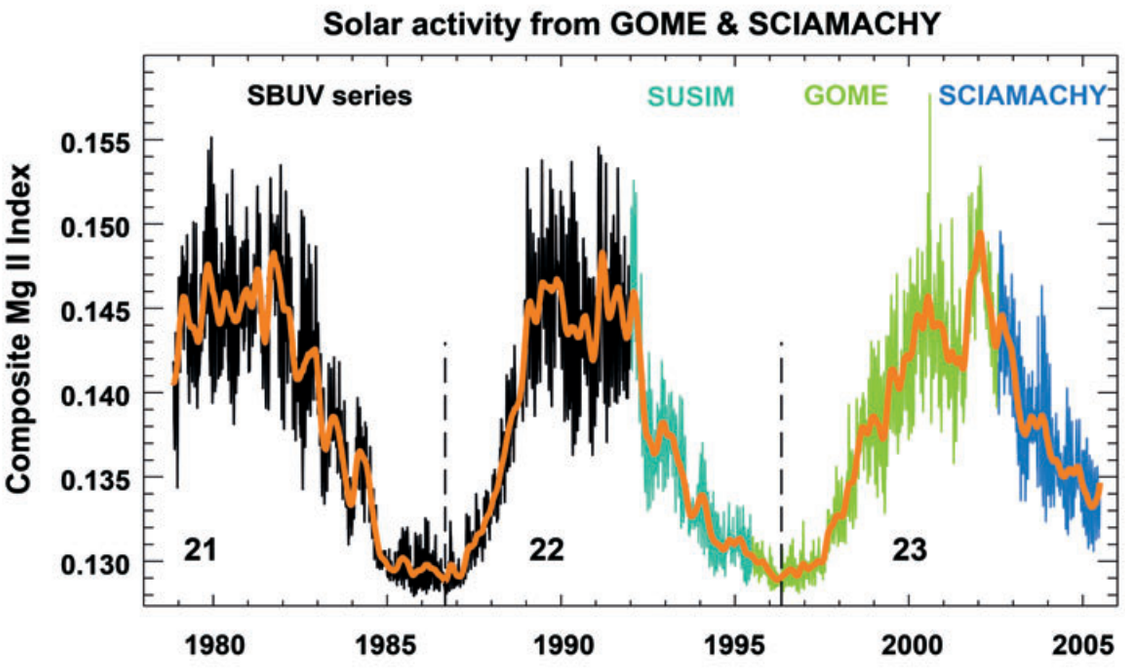

Fig. 10-34: Solar activity measured via the Mg II index by several satellite instruments including GOME and SCIAMACHY. By combining various satellite instruments, the composite Mg II index covers nearly three complete 11-year solar cycles. (graphics: M. Weber, IUP-IFE, University of Bremen)

10.4 Solar Activity

SCIAMACHY's scientific objective to study and monitor atmospheric trace constituents is achieved by analysing solar radiation, both in terms of scattered and reflected sunlight but also in direct viewing for calibration purposes. Due to the high sensitivity and spectral stability it is, in addition, feasible to retrieve information about those aspects of solar activity which manifests themselves in the emitted radiation. Therefore solar observations are analysed on a regular time grid offering the possibility to monitor solar variations. To illustrate how sensitive SCIAMACHY is to variations in the solar flux, fig. 10-33 displays images of the solar disk in white light and the HeII line at 304 Å during high activity on October 28th, 2003 together with the SCIAMACHY signal from channel 3. The large sunspots reduced the effective size of the photosphere which led to a decrease of the measured solar irradiance of about 0.5%.

The Mg II Index

The solar activity shows some well known periodic variations such as the 27 day cycle caused by solar rotation. Another is the 11 year solar cycle, coupled with the 22 year magnetic cycle which correlates with changes in sunspots and Fraunhofer lines. During phases of high solar activity an increase in the number of sunspots in the photosphere and large chromospheric plage areas are observed. The plage areas are hotter than the surrounding areas and cause the enhancement of the emission core within the absorption features of many solar Fraunhofer lines. Thus solar proxy indicators can be given by the core-to-wing ratio of selected Fraunhofer lines. The Mg II index is defined as the core-to-wing ratio of the Mg II Fraunhofer line centered at 279.9 nm. It can be used as a proxy for spectral variations in the solar extreme UV (EUV, *Viereck et al. 2001)* and correlates with atmospheric ozone variations and other relevant atmospheric quantities such as monthly cloud cover (*Svensmark et al. 1997* and references therein).

For the understanding of the solar-terrestrial climate interaction the establishment of long time series covering several solar cycles are important. Due to the limited lifetime of spaceborne missions this has to be constructed from different satellite experiments. Figure 10-34 combines the Mg-II indices for the solar cycles 21 to 23, using data from NOAA missions *(Viereck et al. 2004)*, GOME *(Weber 1999)*, and SCIAMACHY *(Skupin et al. 2004)*. Both the 27 day periodicity and the declining phase of solar cycle 23 are clearly visible. Differences between SCIAMACHY and GOME are mostly below ±0.5%, between SCIAMACHY and NOAA below ±0.25%.

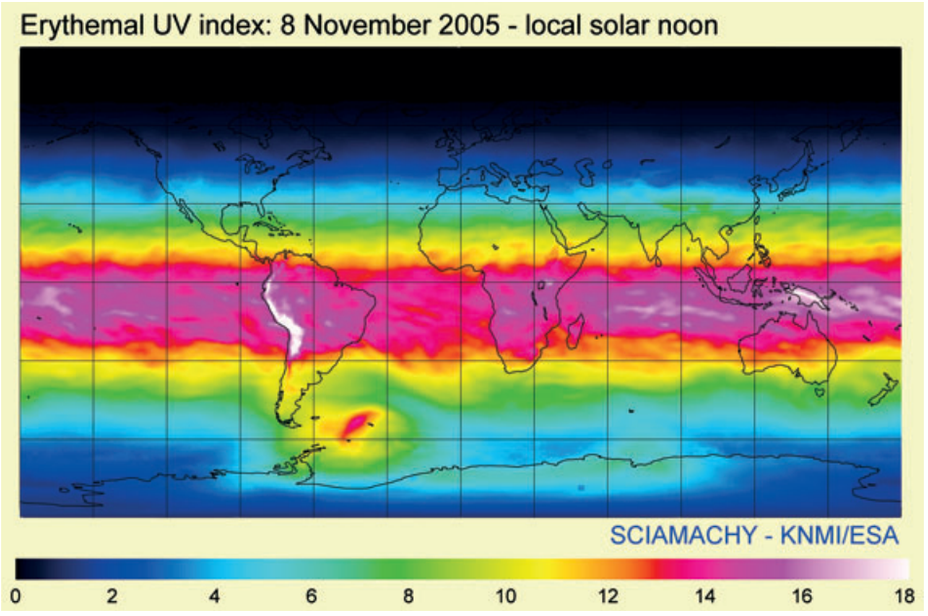

Fig. 10-35: The global UV index on November 8th, 2005. Red denotes high, blue low UV irradiance. (image: KNMI/ESA)

10.5 UV Radiation

UV radiation impinging onto the Earth can be divided into two types: UV-A and UV-B. UV-B is the most active component of sunlight and required by many photochemical reactions. Excessive UV-B may damage flora and fauna. Particularly important for human beings is the fact that UV-B can cause sunburn and may damage human tissue. The amount of UV radiation reaching the Earth's surface depends on ozone concentration, altitude, solar elevation, surface reflectivity, aerosol and cloud cover.

To quantify the UV radiation at the bottom of the troposphere, i.e. our environment, UV related parameters are computed from ozone measurements. These are

- Sunburn times: The time required until skin of a specific type begins to develop sunburn.
- Erythemal UV dose: The amount of UV radiation reaching the Earth taking cloud cover into account, given in kJ/m^2.
- Erythemal UV index: This parameter is the effective UV radiance reaching the Earth's surface under clear-sky conditions given for local solar noon when the sun is highest in the sky. One unit equals 25 mW/m^2. UV dose and index are derived from the assimilated global ozone field at local solar noon.

Several operational services have been established, e.g. at DLR and KNMI, which provide these parameters on a regular basis. Coverage can be global (fig. 10-35), European wide or local (fig. 10-36).

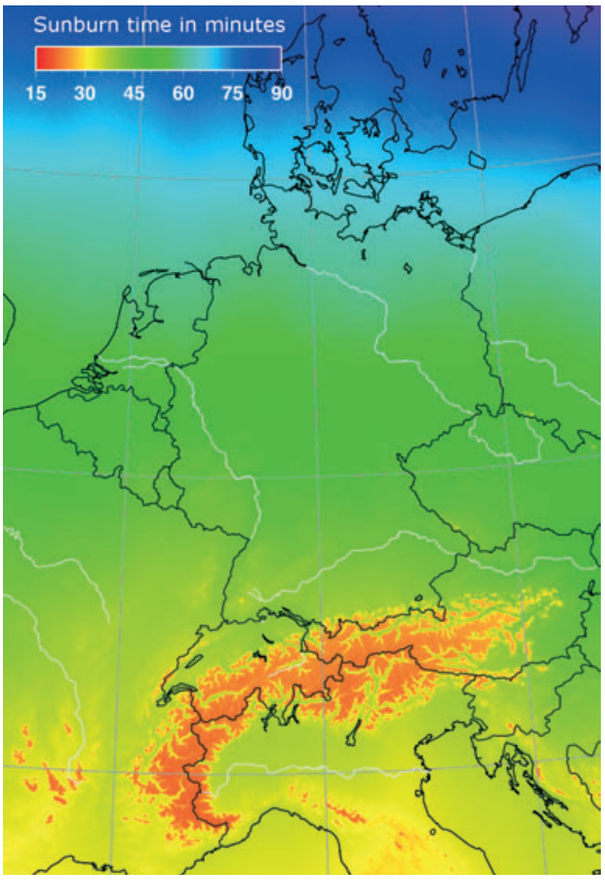

Fig. 10-36: The sunburn time in central Europe in winter. In the Alps at high elevation UV radiation begins to redden skin after only 20 minutes. (image: T. Erbertseder, DLR-DFD)